MODELLING THE GROWTH OF ATLANTIC RANGIA, *RANGIA CUNEATA,* IN RESPONSE TO FRESHWATER INFLOW, TRINITY RIVER DELTA, GALVESTON BAY

by

Mahmoud Eid Ali Amin Omar, BSc

THESIS

Presented to the Faculty of

The University of Houston-Clear Lake

In Partial Fulfillment

Of the Requirements

For the Degree

MASTER OF SCIENCE

in Environmental Science

THE UNIVERSITY OF HOUSTON-CLEAR LAKE

MAY, 2020

MODELLING THE GROWTH OF ATLANTIC RANGIA, *RANGIA CUNEATEA*,

IN RESPONSE TO FRESHWATER INFLOW

TRINITY RIVER DELTA,

GALVESTON BAY

By

Mahmoud Eid Ali Amin Omar

APPROVED BY

_____

George Guillen, PhD, Chair

_____

Cynthia Howard, PhD, Committee Member

_____

Jenny W. Oakley, PhD, Committee Member

RECEIVED/APPROVED BY THE COLLEGE OF SCIENCE AND ENGINEERING:

_____

David Garrison, PhD, Interim Associate Dean

_____

Miguel Gonzalez, PhD, Dean

Dedication

In the hopes that they will be extraordinarily delighted to see me graduating with my Masters' degree, I dedicate this work to my wonderful parents who showed endless support and kindness through my journey. Thank you for your love, encouragement and prayers, you really make my life different. Also, my wonderful kids, Roqaya and Ammar, who I will always do my best to be the father they deserve.

Acknowledgements

Foremost, I would like to express my deepest gratitude to my advisor Dr. George Guillen, and committee members, Dr. Cindy Howard and Dr. Jenny Oakley for their continuous guidance and support. I would also like to acknowledge and appreciate the friendly environment and great experience I had throughout my research assistantship at the Environmental Institute of Houston. And of course, I am indebted to Fulbright Foreign Student Program for giving me the chance to have the experience of studying in United States and going through this amazing cultural and scientific journey.

Thank you all.

ABSTRACT

MODELLING THE GROWTH OF ATLANTIC RANGIA, *RANGIA CUNEATEA*,

IN RESPONSE TO FRESHWATER INFLOW

TRINITY RIVER DELTA,

GALVESTON BAY

Mahmoud Eid Ali Amin Omar
University of Houston-Clear Lake, 2020

Thesis Chair: George Guillen, PhD

Rangia cuneata, commonly known as Atlantic Rangia, is an oligohaline clam found in abundance along the northern Gulf of Mexico. *Rangia cuneata* was selected as one of a suite of indicator species for establishing freshwater inflow regimes in Texas estuaries, including Galveston Bay. Within Galveston Bay, the highest abundances of *R. cuneata* have been in the Trinity River Delta. In the delta, meat index (MI), a health indicator, was found to increase during periods of prolonged freshwater inflow. To build on these results, the primary objective of this study was to model growth of *R. cuneata* in response to freshwater inflow. Ten sites in the Trinity River Delta with historic accounts of *R. cuneata* were equipped with continuous salinity and temperature monitoring devices from February 2018 to August 2019. *Rangia cuneata* were sampled quarterly using two collection methods (hand sampling and clam rake) for abundance, size, and MI. Overall,

559 *R. cuneata* were collected throughout the study. The average MI for the study period was 22 ± 0.32%. Meat index exhibited negative correlation with salinity and sediment percent fines. *Rangia cuneata* shells were examined to evaluate the influence of environmental conditions on shell growth and determine the shells age. Shell index (shell weight/ total shell dimensions (length + width + height)) is a new growth index suggested as a long-term health indicator. *Rangia cuneata* were aged based on winter marks in outer shell layer. Measured age along with length data were fitted in von Bertalanffy growth model. The output function of the model was rearranged and used to measure age of all collected *R. cuneata* (n = 599) throughout the study based on their length data. The Trinity River Delta had a growing population with majority of individuals at 3-4 years old and the oldest individuals were 6.5-7 years old. Shell growth represented by both annual growth bands width and annual increase in height was higher in years with higher average freshwater inflow. *Rangia cuneata* has been shown to be a responsive indicator species to multiple metrics that are directly related to freshwater inflows within the Trinity River Delta. While meat index is a short-term metric to measure *R. cuneata* health, shell growth (measured by shell index) is a better metric to understand long-term growth and health. Continued growth and health monitoring using multiple techniques are suggested to better understand *R. cuneata* response during periods of low flow.

TABLE OF CONTENTS

LIST OF TABLES

LIST OF FIGURES

INTRODUCTION

Literature Review

Distribution of *Rangia cuneata*

Atlantic Rangia, herein called *Rangia cuneata* or clam(s), is an estuarine to brackish water clam found from New Jersey on the U.S. Atlantic coast extending through the Gulf of Mexico (GOM) to the Laguna de Terminos, Campeche, Mexico (LaSalle et al. 1985). *Rangia cuneata* is present in at least 16 estuaries along the GOM (Wakida-Kusunoki and MacKENZIE Jr, 2004) and is abundant within the mouths of coastal rivers and bayous. *Rangia cuneata* exhibits maximum growth rates in brackish water where optimum salinity conditions for growth and reproduction occur (Parnell et al., 2011).

Johns (2012) studied factors that appeared to limit the occurrence and distribution of *R. cuneata* in the Guadalupe and Mission-Aransas estuaries in Texas. He deployed a novel approach to study the relationship of salinity exposure and the occurrence of *R. cuneata* by integrating salinity magnitude, duration of occurrence and periodicity of re-occurrence. Among his findings, he concluded that favorable conditions for reproduction and recruitment of *R. cuneata* are more frequent in upstream portions of the examined estuaries and drop off towards the higher-salinity portions toward the open bays. However, Johns (2012) pointed out that the relationship between salinity patterns and *R.cuneata* population distribution is complicated and the strict salinity range required for survival of larvae and successful recruitment does not have to be met to maintain a viable population since adult clams are more tolerant to higher ranges of salinity (Johns, 2012).

Parnell et al. (2011) compared the distribution of *R. cuneata* in different portions in Galveston Bay exposed to different levels of freshwater inflow including low salinity Upper Bay sites (Trinity River Delta, Trinity Bay and Clear Lake) and higher salinity

East Bay sites. During their study, they found that the average meat index (MI) and shell length of *R. cuneata* collected from Upper Bay sites were significantly higher than those of *R. cuneata* collected from the East Bay sites where exposure to freshwater inflow was lower.

Spawning and early stage growth

LaSalle et al. (1985) reviewed the literature on *R. cuneata* reproduction cycle in different estuarine systems found in Virginia, Florida, Louisiana and Campeche, Mexico. In both Louisiana and Florida, *R. cuneata* was reported to spawn twice a year, around springtime and late summer/fall time.

Cain (1973) studied the spawning of *R. cuneata* in the laboratory by observing the combined effects of temperature and salinity on survival and growth of fertilized eggs and veliger larvae. His results showed that the optimum ranges for maximum (85%) embryo survival were 18 °C to 29 °C and 6 to 10‰ for temperature and salinity, respectively. They concluded that early embryo development was affected more by salinity than temperature. Optimum conditions for the survival and growth of larvae (8° - 32°C; 2 -20 ‰) were broader compared to embryos (6-10 ‰) (Drescher 2017). However, lowest survival was observed at low salinity-high temperature and high salinity-low temperature conditions. Highest growth of larvae occurred at high salinities and high temperatures (Cain, 1973).

Ecological importance

Rangia cuneata is a non-selective filter-feeder that can constitute about 95% of benthic biomass in GOM coastal water (LaSalle et al, 1985). Due in part to its high abundance, *R. cuneata* has been documented to be a significant prey item to a wide range of fishes, crustaceans and wading birds (Cain, 1975; LaSalle et al., 1985; Wong et al., 2010). Since *R. cuneata* growth is influenced by variation in freshwater inflows and

salinity into estuaries, it has been degsignated as one of the primary indicator species for establishing freshwater inflow regimes in Texas estuaries by the state of Texas (Johns, 2012).

Rangia cuneata aging

Several approaches have been used to age *R. cuneata* depending on structure of shell. The most simplistic approach utilized the number of annual growth increments (rings) on the external surface of the shell to estimate age and growth rate (LaSalle and de la Cruz, 1985; Tenore et al., 1968).

Black and Heaney (2015) used a different approach to age *R. cuneata* that is based on defining the annual growth increments in the shell sections. One annual growth increment is a combination of two adjacent layers under light reflection; a dark layer that represent active growth during spring and summer, and translucent layer that represents slow growth during fall and winter (if any). The only limitation of Black and Heaney's approach is that they did not consider the early partially completed first (year of origin) and last (year of death or collection) that in total may add up to one year to their total age.

The more detailed approach for aging was used by Fritz et al. (1990). His method utilized structure of the shell layer to determine age with the justification that growth patterns in the outer shell layer is proved to be more reliable than those in the inner layer. Inner layer growth patterns are reversible and can be subject to decomposition under anaerobic conditions (anaerobiosis) caused by prolonged shell closure (during drought or unusual cold weather) (Fritz et al., 1990; Surge and Schöne, 2015).

Freshwater inflow management in Galveston Bay

Galveston Bay is a unique and productive estuarine system located in Southeast Texas. It is one of the most ecologically and economically important estuarine systems found within the GOM (Ko and Johnston, 2007). Trinity River Delta (TRD) where the study was conducted is the entrance through which freshwater from Trinity River inflows into the Trinity Bay to blend in Galveston Bay. Additionally, San Jacinto River, coupled with Trinity River, known as Trinity-San Jacinto estuary, are two of three major sources of inflow discharged in Galveston Bay. The San Jacinto River annually discharges 616.5 m3 to the bays in average while the Trinity River annual median discharge is 9,247.5 m3 (Pulich Jr, 2007).

This freshwater inflow is of crucial importance to maintain sufficient levels nutrients and transported sediment and to keep salinity in the bay within limits that support the diversity of biological communities and keep the ecosystem in a healthy state. With increasing development along Trinity River and associated watershed in addition to alternating periods of drought and heavy rain, it is critical that sound science based environmental management strategies be developed for this estuary. Texas Senate Bill 3 (SB3), enacted by Texas legislature in 2007, mandated the development of strategies to establish and monitor freshwater inflow standards in order to estimate the amount of freshwater inflows necessary to maintain the ecosystem health of Texas bays and estuaries (Quigg and Steichen, 2015).

Texas Senate Bill 3 mandated the development of strategies to establish and monitor freshwater inflow standards in order to estimate the amount of freshwater inflows necessary to maintain the ecosystem health of Texas bays and estuaries (Quigg and Steichen, 2015). The bill amended the Texas Water Code (TWC) §11.1471 that requires the Texas Commission on Environmental Quality (TCEQ) to adopt appropriate

environmental flow standards for each river basin and bay system in the state that will adequately support a sound ecological environment (TSJ-BBEST, 2009). It also established a stakeholder-based process to consider environmental flow needs in new water rights permits.

The Trinity-San Jacinto Basin and Bay Expert Science Team (TSJ-BBEST), a multidisciplinary team of scientists, was created by Basin and Bay Area Stakeholder Committee (BBASC) to recommend environmental flow regimes for the Trinity River, the San Jacinto River, and Galveston Bay in addition to selecting a list of key indicator species (Parnell et al., 2011; BBASC, 2012).

Quigg and Steichen (2015) evaluated the list of potential bioindicators developed by the TSJ-BBEST in addition to some other fish and invertebrate species. *Rangia cuneata*, one of the listed species, was evaluated based on the Texas Parks and Wildlife department data for bay trawl catch from 1980 through 2010. Although the bay trawl weren't specifically designed to catch *R. cuneata* (they were collected as by-catch), the bay trawl data was the most comprehensive time series data available, therefore, it was used for analysis. They concluded that an increase in abundance was correlated with increase in salinity ($p<0.05$) in Trinity Bay and Upper Galveston Bay.

Recent surveys for *R. cuneata* abundance in Galveston Bay

In addition to the TSJ-BBASC recommendations based on a historical review of data by Quigg and Steichen (2015) that utilized available historical data, Parnell et al. (2011) surveyed *R. cuneata* in Galveston Bay from October 2010 to August 2011 using more appropriate methods (hand sampling, trawling and oyster dredge) with the objective of determining the distribution of *R. cuneata* in relation to salinity gradients in Galveston Bay. Using a non-repetitive monitoring design, they sampled 92 sites throughout Trinity Bay, Upper Galveston Bay and Lower Galveston Bay. The severe drought that occurred

during the study period, as stated by Parnell et al. (2011), decreased freshwater inflow into Galveston Bay and therefore may have severely biased the understanding of the spatial distribution of *R. cuneata* and its response to freshwater inflow. Therefore, one of the main recommendations and future goals of this study was to repeatedly monitor water quality parameters and collect *R. cuneata* samples at a few stations within each survey area on a monthly basis.

More recently**,** the Environmental institute of Houston (EIH), funded by the National Wildlife Federation (NWF), surveyed *R. cuneata* in the TRD and associated bayous and sub-bays with additional sites monitored during January and February 2016 when higher riverine inflows occurred. From this study, Guillen et al. (2016) concluded that the MI (the ratio of wet soft tissue weight to total weight, MI%) had increased compared to former levels reported in 2010-2011 study. Based on comparison of these studies it appears that *R. cuneata* collected during 2016 study during wetter conditions contained proportionately more soft tissue for all shell sizes. The increase in freshwater inflow likely reduced stressful conditions due to high salinity that existed during the drought years of 2011-2014 (Guillen et al., 2016). Average salinity and MI from these studies show the MI increases with the decrease in salinity due to higher freshwater inflow (Table 1).

Table 1. Summary of previous recent studies on *R. cuneata* in Trinity Bay.

Study	**Duration**	**Number of sites**	**average salinity (psu)**	**Average MI (%)**	**Average length (mm)**
Parnell (2011)	Oct 2010- August 2011	27	> 12	12.5	55.7
Windham (2015)	October 2011- November 2014	5	7.6	11.5 (2012) - 11.2 (2014)	47.29 (2012) - 49.46 (2014)
Guillen (2016)	January- Feb 2016	50	0.4	30.3	47.7
Current study	February 2018 - July 2019	10	1.06	22	56.25

Study objectives

The primary objective of this study was to compare the growth and health of *R. cuneata* in the TRD of Galveston Bay to freshwater inflow and associated salinity. To achieve this objective, *R. cuneata* abundance, size distribution, MI (as a health indicator), and shell growth were evaluated in response to freshwater inflow. Shell structure analysis was used for age determination in addition to observing the effect of different inflow regimes on shell growth rate.

Data collected during previous surveys including freshwater inflows, salinity, varying drought/rain conditions and distribution patterns of *R. cuneata* were used (whenever relevant) to compare with results generated from the current study.

METHODS

Study area

This study was conducted throughout the TRD. Ten sites were selected from sites sampled during a previous survey (50 sites established by EIH, during January and February 2016) based on the occurrence and abundance of *R. cuneata* in the TRD. Current study sites were either located on the main channel of Trinity River, Delta tidal creeks, or the open Triniy Bay (Figure 1) and (Table 2)).

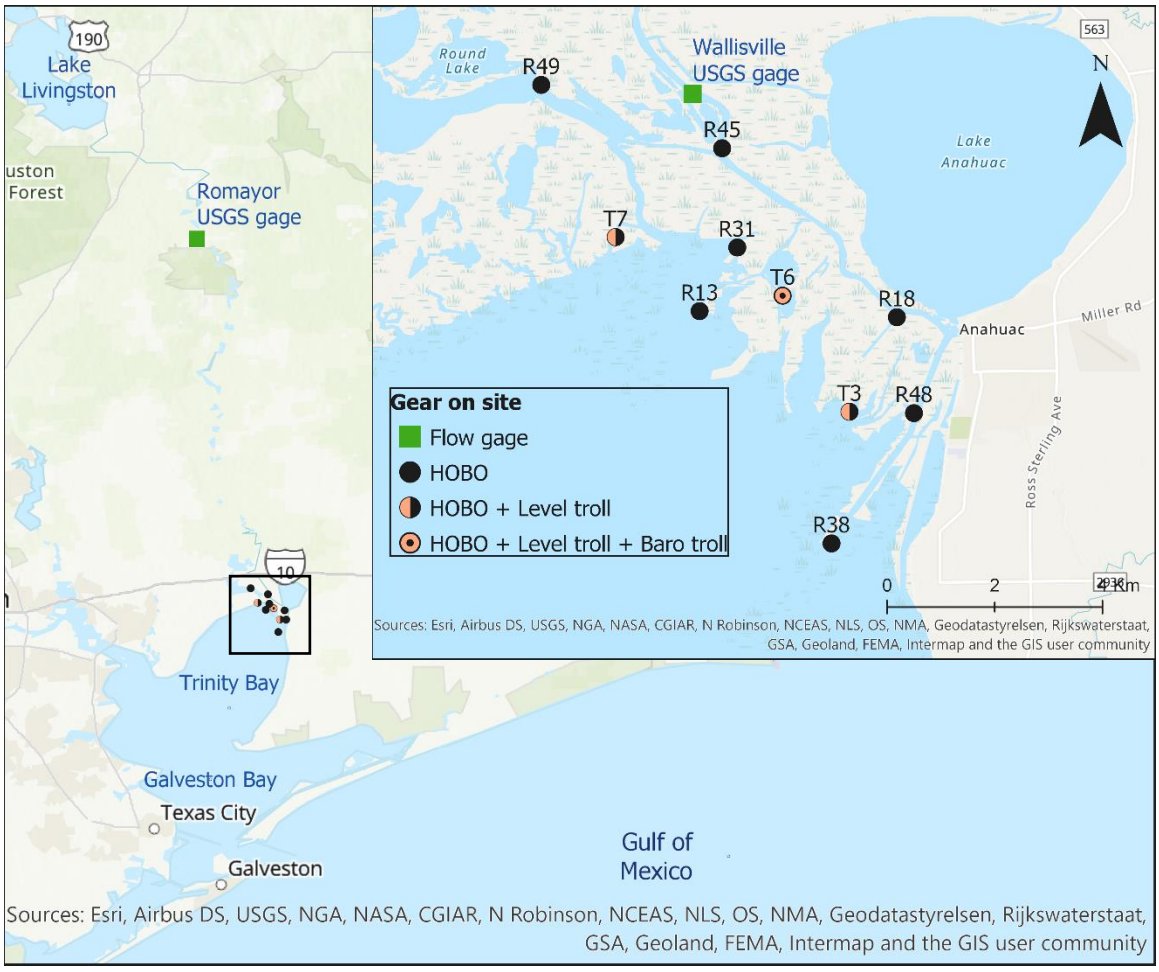

Figure 1. Distribution of sampling sites for *R. cuneata* throughout the Trinity River Delta.

Table 2. Sampling sites locations (latitude and longitude) and on-site installed gear.

Site ID	Latitude	Longitude	On-site gear
R18	29.77493	-94.69698	HOBO data logger
R38	29.73719	-94.7079	
R48	29.75893	-94.69413	
R13	29.77595	-94.72993	
R31	29.78657	-94.72364	
R49	29.8137	-94.75638	
R45	29.80313	-94.72617	
T3	29.75916	-94.70491	HOBO data logger + Level TROLL
T7	29.78830	-94.74395	HOBO data logger + Level TROLL
T6	29.77853	-94.71607	HOBO data logger + Level TROLL + Baro-TROLL

Study sites were distributed throughout the TRD. Some sites were located directly on the main channel of Trinity River (R45, R18 and R48). Some other sites were located on bayous and shallow streams within the delta (T6 and T7) while some sites faced the open bay (R38 and R13). Freshwater inflow data for this study were measured by USGS gages on Trinity River at located upstream at Romayor (08066500) and downstream near the TRD at Wallisville (08067252) in cubic feet per second (cfs). Old River which inflows in TRD as receives freshwater as a diversion (overbank outflows during high freshwater inflow events) from Trinity River between Romayor and Wallisville gage. Site 49 was located in the Old River where freshwater inflow was not continously monitored.

Field work

Rangia cuneata sampling

Sampling for *R. cuneata* was conducted as part of a project under contract with the Texas Commission on Environmental Quality (TCEQ) with the contract name "Characterization of the influence of freshwater inflow on TRD indicators" and number "582-18-80338". To achieve the objectives of this study, quarterly sampling for *R. cuneata* was conducted at the 10 study sites with a total of six sampling events. Sampling events were conducted during April, July and November 2018; and January, April and July 2019.

All sampling sites were located in shallow (< 1m) water along shorelines and tidal creeks. A combination of modified clam rakes and hand sampling were used to sample *R. cuneata* at each site. The clam rakes used during the study measured 35 cm width, 14.6 cm depth and 22.9 cm height with 8.3 cm teeth length, and 2.5 cm gap distance between teeth. The rake basket was lined with 1.3 cm square wire mesh and was controlled by a 190 cm handle. Clam rakes were pulled for 30 seconds (3 replicates per site). Hand sampling was conducted by hand digging in sediment to about 30 cm depth in area of 1 m^2 (3 replicates per site).

Catch from different gears and replicates were kept separate. Both live and dead but whole (both valves connected) *R. cuneata* were collected. When possible, up to total 20 individuals were retained from each site during each sampling event for further lab morphometrics and MI determination. In case the six replicates of rake and hand sampling combined did not yield 20 clams, random digging for clams (defined as "opportunistic") was conducted to complete the targeted 20 clams. During November 2018, only 5 sites were sampled for *R. cuneata,* while the other sites were impossible to sample using our standard protocol due to high water levels encountered during this time.

Sediment sampling

One sediment sample was collected from each site during each sampling event. Depending on sediment type, a Petite ponar (length = 15.2 cm; width = 21 cm) or Ekman dredge (length x width = 15.2 x 15.2 cm) were used for sampling. Target sediment sample depth was 10 cm. Samples were retained for percent fines analysis in the lab. Only 5 sites were sampled for sediment on November 2018 sampling event and data from these sites were not used in analysis.

Water quality and water level monitoring

Onset® HOBO® data loggers were used for logging temperature, conductivity and salinity at 15 minute intervals. HOBO gear was retrieved monthly for maintenance and data retrieval. During data retrieval, side by side measurements were performed using the YSI® ProDSS Sonde to measure temperature (°C), conductivity (µS) and salinity (psu). The ProDSS Sonde measurements were used to validate and calibrate the HOBO data. Other environmental variables were measured during sampling events including dissolved oxygen (DO mg/l), Secchi tube for clarity (m) and pH. These variable were measured as grab samples using YSI® Pro DSS Sond (DO and pH) during *R. cuneata* sampling events.

Water level instruments (In-Situ Level TROLL) were installed at three sites for continuous water level monitoring (Table 2). An on-site In-Situ Baro-TROLL was deployed at the T6 site to continuously monitor barometric pressure, which was used to correct the Level TROLL readings.

Laboratory Analysis

Morphometrics and health metrics

Morphometrics including shell length, width and height in (mm) were measured for all retained *R. cuneata*. Different axes for morphometric measurements of *R. cuneata* shells that were used include: length (L) from anterir to posterior edge of shell; height (H) from umbo to the ventral edge of the shell; and width (W) through the thickest shell transect (Figure 2). In addition, total dimensions of the shell, henceforth refered as TD, was calculated as the total of dimensions (L + H + W). For health metrics, 10 living whole clams (with soft tissue inside) from each site were used to assess the MI. During MI assessment, each clam was 1) slightly shucked to drain any retained water then weighed as whole, 2) completely shucked using an oyster shucking knife from the umbo side and soft tissue (meat) removed, then 3) the empty shell was weighed, respectively. The MI was calculated as following:

$$\text{Meat Index (MI)} = \frac{\text{Soft tissue weight}}{\text{Whole weight}} \times 100$$

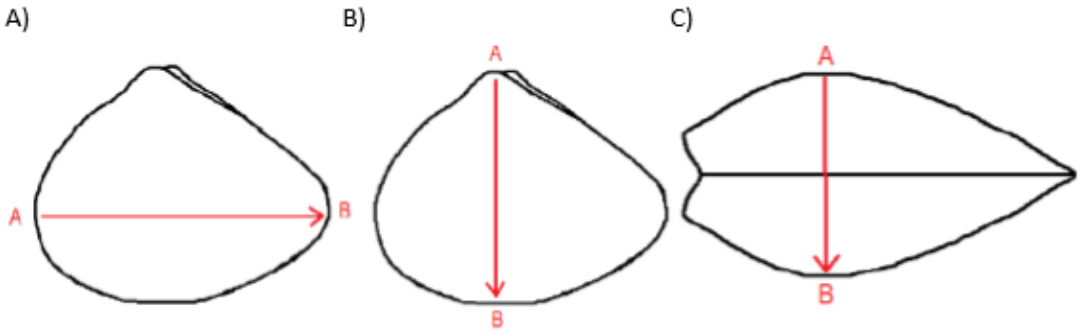

Figure 2. Measurement axes of shell morphometrics. A) Length, B) Height and C) Width. (Guillen et al., 2016).

Sediment percent fines analysis

Sediment samples were measured for percent fines as a method to determine the dominant sediment particle size and observe the spatiotemporal change in sediment composition. Composition of fine sediments from each site were calculated using protocol described by Ginn et al. (1990). Sediment samples were homogenized in the sample bag. Fifty milliliters (ml) were taken and passed through a #63 sieve to rinse off fine sediments. Remaining sand and larger grains were then placed in a 100mL graduated cylinder and topped off with water. After the sample was allowed to settle out for 5-10 minutes, the volume of sand and larger grains was recorded. Percent fine composition was calculated as following:

$$\text{Fines } \% = \frac{\text{Initial sample volume}(50 \text{ ml}) - \text{Volumeof remaining}}{\text{Initial sample volume } (50 \text{ ml})} \times 100$$

Shell sectioning and aging

Bivalve shells have two major orientations: dorsal-ventral and anterior-posterior aspects. The dorsal region (umbo) is the oldest growth as the shell continuously grows outward, extending to the ventral region where the active, growth takes place (Drescher, 2017). *Rangia cuneata* shell morphology is characterized as having equivalves (two identical valves) that are inequilateral (where the umbo points toward the anterior part of the shell) (Figure 3). Right and left valves were measured from the posterior aspect of the shell (LaSalle et al., 1985; GISD, 2020). Shell sectioning was conducted for two main objectives; to measure the growth rate using the outer and inner shell layer and to determine actual age based on annual growth marks in outer and inner layers.

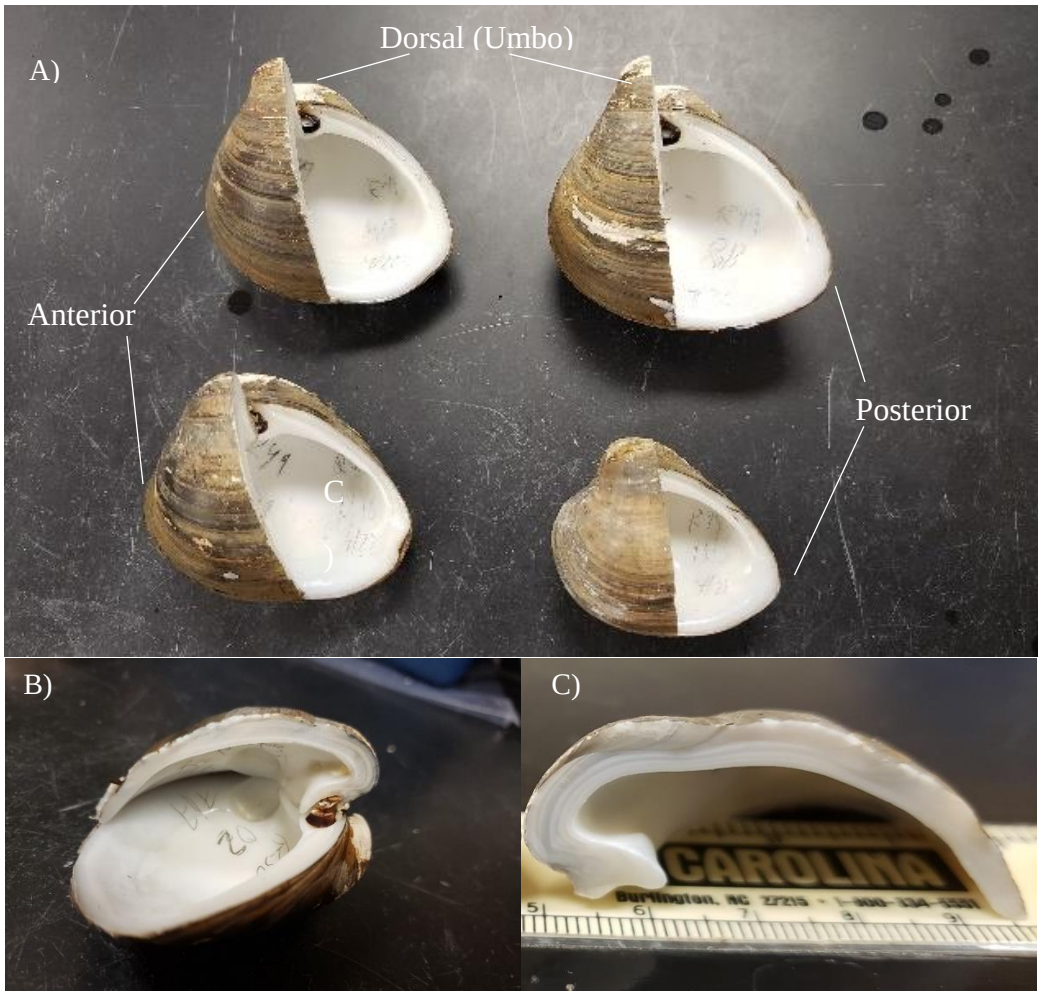

Figure 3. Shells processed for aging by annual increment visualization. A) Cutting axis through clam shells (missing part is the part used for aging). B) Side view of sectioned valve (posterior view). C) Valve-half cut and ready for sanding and polishing.

Rangia cuneata shells from different sites, size ranges, and water conditions were cross-sectioned with the purpose of visualizing the growth bands throughout the inner layer and, more importantly, locating winter marks through the outer layer to be used as the key marks for accurately aging the examined shells following methods described in Fritz et al. (1990). For shell sectioning purposes, a tile saw (SKIL 3540-02) was used to wet-cut the left valve into two (unequal) halves through the longest axis from the umbo to the ventral edge of the valve (the clam's bill) (Figure 3). This axis is the same axis where the height of clam was measured. The face of the cut for the posterior half of the

left valve was then sanded and polished using belt and disk sanding machine (WEN 6502T).

For initial sanding, sectioned shells were sanded against a gradient of sanding belts with 600, 800 and 1000 grit (one minute sanding on each followed by rinsing with deionized water) to ensure fine sanding without damaging the sectioned shell. Following sanding, a gradient of 3000, 5000 and 7000 grit discs were used to polish the section surface (two minutes polishing with each grit level followed by rinsing with deionized water). Sectioned shells were allowed to air dry before visualization.

A stereomicroscope system (OLYMPUS SZX16) with an installed high resolution color camera (OLYMPUS DP73) was used to examine and photodocument polished shell sections. For microscopic examination, shell halves were fixed under the microscope by holding the specimens in Petri dish full of glass beads. Polished sections were visualized through light reflected on the section, photographed by the camera and then processed by the OLYPUS cellSens software. Winter marks and width of growth bands of each shell were measured. The shell measurement data was then recorded in a project database. The image was also saved with measurment axes and scale bar as a reference.

During this study, shell sections were examined for both growth bands in inner and winter marks in outer shell layers. While examining, matching inner layer growth bands with outer layer winter marks was ensured. Two categories of data were recorded for each shell, the outer layer winter marks data and inner layer annual growth bands data. Defining and locating winter marks used to measure height of the shell at a given winter.

Winter marks throughout the shell outer layer were defined and located according criteria developed by Fritz et al. (1990). A winter mark is an annualy formed thin layer of translucent microstructure material that results as growth slows during winter due to low temperatures (Figure 4). The distance from the umbo peak to each winter mark was measured (Figure 2 and Figure 3) ; this measurement is essentially the shell height during that winter (Figure 4 and Figure 5).

Most shells (shells with height 25 millimeters (mm) or more) were too large to fit within the microscope field as whole to measure height at different winter marks. To measure the distance from umbo to winter marks in these shells, a caliper (sensitivity = 0.1 mm) was used by positionig the tip of the caliper arm on the winter mark (under microsope to ensure fitting of caliper on the winter mark) and the other arm of caliper at the umbo peak. Height in mm at winter mark data was recorded for subsequent growth analysis.

Annual growth in the shell inner layer is demarcated by by the alternation of dark and light bands formed in spring/summer and fall/winter. The growth band, known as "annuli", were counted and measured for thickness as illlustrated in Figure 4). Annuli thickness was measured and was later evaluated as a health indicator by estimating its spatiotemporal variation and correlation with freshwater inflow for the corresponding years.

The number of winter marks was used to estimate the number of the complete years of growth the clam lived. Complete year of growth means the full year from spring to winter the clam lived and henceforth will be refered as year of growth . An example illustrated in Figure 5) of a shell with 3 winter marks most likely lived 2 years.of growth In addition to the years growth of the clams lived, the early growth before 1st winter mark (i.e. The early growth took place since the recruitment through the first winter) and the late growth after the last winter mark need to be identified and assessed (Figure 5).

Early growth prior to the 1st winter mark, was measured by the height at the 1st winter mark. A histogram of height data was then plotted. The frequency distribution was examined for bimodality (because they are known to spawn twice per year) and individuals were then classified into spring or fall recruits based on mathematical cutoff calculated based on bimodal distribution of data of measured height at first winter mark. Spring recruits were assigned a full year age for the early growth period and fall recruits were assigned a half a year for the early growth.

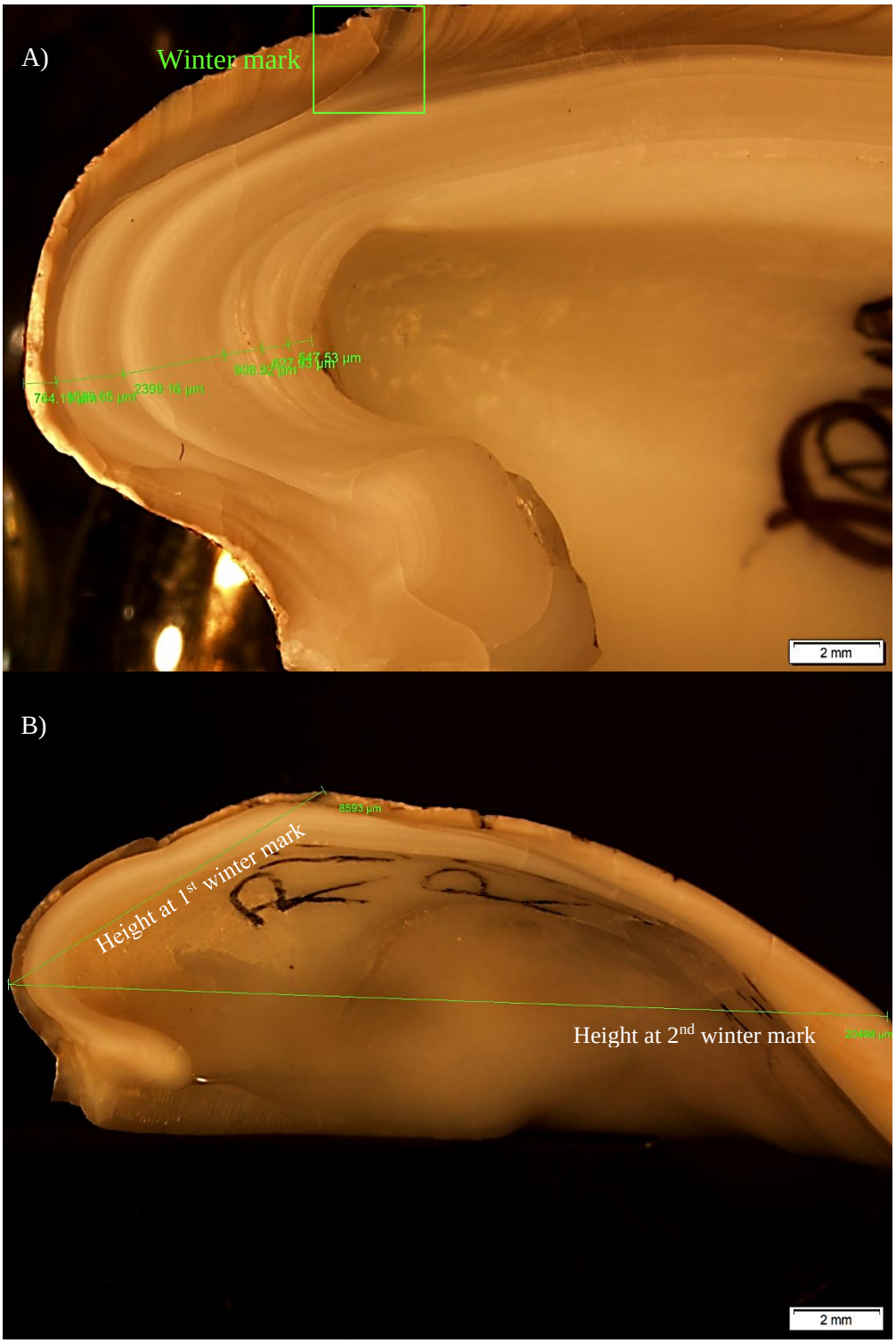

Figure 4. Shell sections visualized and measured for A) Width of annual growth bands at the shortest axis from peak of umbo to the corresponding point at the interior of the shell. B) Height from peak of umbo to the winter mark.

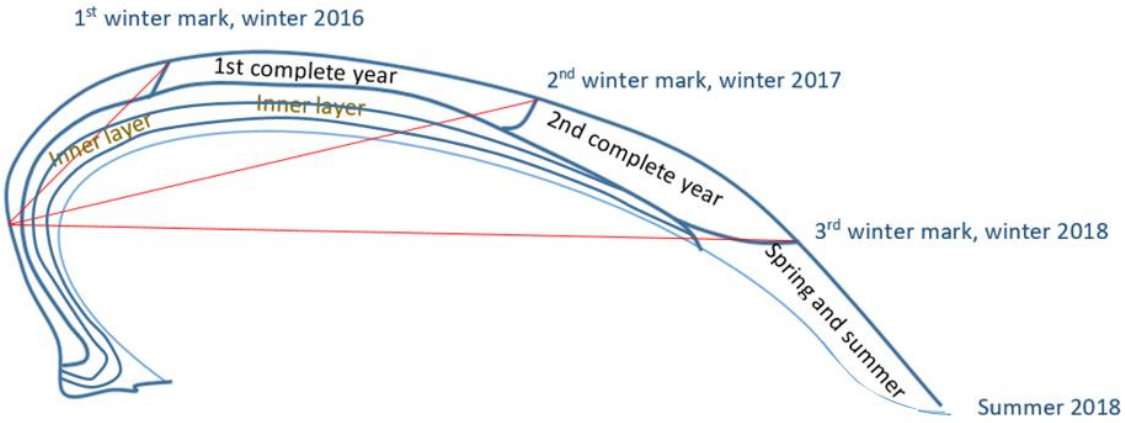

Figure 5. Illustration showing the structure of the shell and location of winter marks for a shell collected on summer 2018 and assessed to be recruited in either spring or fall 2015.

The age of the late growth period after the last winter mark was determined based on the sampling event. *Rangia cuneata* collected in spring (April) were assigned quarter a year while *R. cuneata* collected in summer (July) were assigned half a year for the late growth. Total age of a given shell, reported to the quarter year, is calculated using the following equation:

$$\text{Total age} = \text{Early growth} + \text{Completed years of growth} + \text{late growth}$$

Data analysis

Summary statistics were generated (in Microsoft Excel) and compiled for freshwater inflow, salinity and temperature for different time steps (preceding 30, 60, and 90 days prior to each sampling event). This was done to evaluate the effect of flow regimes over different time periods on temperature and salinity and on the somatic growth of *R. cuneata* collected during each sampling event.

To measure its effect on MI, salinity was statistically summarized as average daily salinity magnitude (DSM) for 30, 60 and 90 days prior *R. cuneata* collection. Average DSM is the average value of the daily range of salinity (= Maximum - minimum salinity value for a given day). Average daily salinity magnitude, DSM, has an advantage over the average salinity for the same period. Average DSM implies the daily fluctuation in local site salinity, i.e. Sites with higher average daily salinity magnitude were more likely to have higher daily fluctuation in salinity and vice versa. Also, MI data were statistically summarized as median MI per site/sampling event to avoid the effect of outliers.

Linear correlation analysis, using Microsoft excel, was conducted between local salinity measurements and freshwater inflow to determine if there was a linear relationship between inflow and the local salinity at each site. Sediment percent fines were tested for variation among sites. The relationship between the sediment percent fines and preceding freshwater inflow (as measured at the Wallisville gage) were analyzed using linear correlation. Also, correlation between MI and environmental variables were tested. Significant ($p<0.05$) correlations (r) between variables were reported in tabular format.

Simple and multiple linear regression models, using Microsoft Excel, were also used to test and measure the potential relationships between physiochemical and

biological continuous scale variables. Multiple regression analysis was used to test the combined effect of salinity, sediment percent fines and temperature on MI. Statistical parameters (coefficient of determination, R^2, p value and line equation) from regression analysis tests were listed in results and the detailed statistical output from regression tests were provided in the appendix.

Additional statistical tests were employed to examine spatial-temporal patterns in physicochemical and biological variables between different levels of categorical variables (e.g. sites, months). Prior to analysis, the data was tested for normality, in PAST v 3.26, using the Anderson-Darling (Razali and Wah, 2011). If the data from the examined groups were not normally distributed, exhibited equal variance or the sample size was not large enough (with outliers), non-parametric tests were used (Scheff, 2016).

The Kruskal-Wallis ANOVA Test for equal medians (McKight and Najab, 2010) and Mann-Whitney Pairwise Test (MacFarland and Yates, 2016) were performed in PAST v 3.26 software. Kruskal-Wallis was basically to detect if any significant differences between samples medians. Kruskal-Wallis test output statistics were provided in the appendix.

Mann-Whitney test results were plotted using boxplots to illustrate the median of different samples. Confidence intervals were plotted as “notches” around the median line on the box (Figure 6). If two boxes' notches do not overlap there is ‘strong evidence’ (95% confidence) their medians differ (Chambers, 1983).

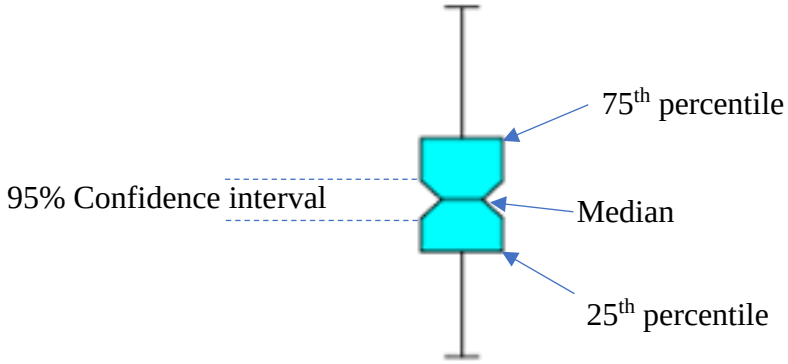

Figure 6. Illustration of "Box" with median, 25th percentile, 75th percentile and 95% confidence interval.

Also, violin plots were used, overlapping the boxplots, to illustrate the frequency distribution of shell size per sites and sampling events.

The statistical significance for all Mann-Whitney pairwise tests of variables between categories (e.g. site or sampling event) were subsequently reported in tabular format with additional output statistics from Mann-Whitney Pairwise test (Mann-Whitney U, samples size, N, and median) were provided in the appendix.

To simplify the complexity of high-dimensional environmental data, Principal Component Analysis (PCA) was employed (Lever et al., 2017). Correlation-based Principal Component Analysis (PCA) test was applied to predict correlated environmental variables in relation to MI. PCA analysis was performed in PAST v 3.26 software.

Based on PCA analysis, MI data were further tested for correlation (in Microsoft Excel) with salinity, sediment percent fines and other environmental parameters. This correlation was tested on the sampling event level and the whole study level as well.

Shell microscopic examination data were initially collected as records of heights at winter marks and widths of annual growth bands for each clam. Early growth data of *R. cuneata* shells were tested for the presence of bimodal distribution using a finite

mixture model that utilizes expectation–maximization algorithm to estimate the cutoff height between spring and fall recruits. To test the bimodality and estimate the cutoff, packages “devtools”, “EMCluster” and “cutoff” were used in open source R studio.

The relationship between shell length and determined age data was modelled using a von Bertalanffy growth model to develop at predictive length at age model (Fabens, 1965). Age and size data were fitted in von Bertalanffy growth model using PAST v 3.26 software. The von Bertalanffy growth function (VBGF) was calculated using the Fabens (1965) equation as following:

$$L = \mathrm{L}_{\infty} * (1 - b * e^{(-k(t))})$$

Where:

L is the length of the clam to be aged.

L_{∞} is the average size at the maximum age (assuming they grow to infinity).

b is calculated from the equation: $\mathrm{b} = (\mathrm{L}_{\infty} - L_0)/\mathrm{L}_{\infty}$

k is the growth rate coefficient, a measure of how quickly L_t approaches L_{∞}

t = age of clam with known length

This output formula from the model was rearranged to measure age (t) from length (L). Rearranged formula to calculate age (t) is:

$$t = \frac{\ln(L_{\infty}) + \ln(b) - \ln(L_{\infty} - L)}{K}$$

Other software used for data analysis and plotting are ArcGIS Pro and ArcMap 10.4.1. ArcGIS Pro was used for sites mapping based on coordinates and ArcMap was used for plotting abundance per sites.

RESULTS

Environmental variables

Freshwater inflow and local site salinity

An inverse relationship between freshwater inflow and local salinity levels was observed upon visual examination of line graphs depicting freshwater inflow versus local salinity levels measured at each study site (Figure 7). Highest salinity levels at each site generally occurred during time periods exhibiting the least amount of freshwater discharge (Figure 7). However, the magnitude of salinity readings between sites varied based on their geographic proximity to the freshwater inflow from the Trinity River and Old River.

Local salinity measured at the different sites responded differently to fluctuations in discharge from Trinity River. Sites located on the mainstream of Trinity River (R18 and R45) recorded the lowest average salinity during the study period. In contrast, maximum and average levels of salinity were highest at sites in the lower portion of the delta (i.e. R38 and T7) which were more exposed to open bay tidal fluctuation and salt water intrusion less influenced by the freshwater inflow (Table 3).

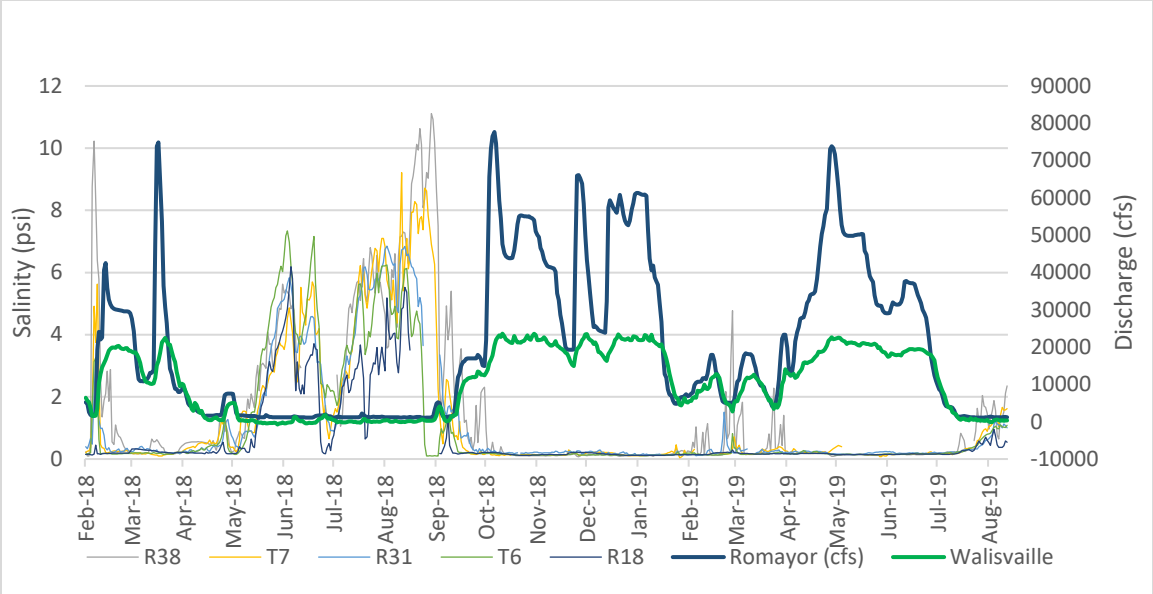

Figure 7. Relationship between discharge (at Romayor and Wallisville in thick dark blue and green lines, respectively) and the local salinity recorded simultaneously by HOBO data loggers at 5 selected sites with 1st, 3rd, 5th, 7th and 9th highest average salinity).

Table 3. Table of local salinity summary statistics from each of the study sites.

Site	Min.	Quartile 1	Median	Mean	Quartile 3	Max.
R38	0.07	0.14	0.19	1.47	1.46	12.28
R13	0.10	0.15	0.19	1.45	1.06	14.44
T7	0.01	0.16	0.22	1.28	1.13	15.80
T3	0.09	0.17	0.22	1.20	1.01	10.75
R31	0.10	0.19	0.24	1.12	0.90	7.89
T6	0.09	0.14	0.18	1.05	0.67	8.58
R49	0.04	0.16	0.20	1.07	0.62	8.14
R48	0.10	0.14	0.17	0.95	0.44	12.37
R18	0.08	0.15	0.18	0.67	0.27	6.34
R45	0.07	0.14	0.17	0.54	0.25	7.18

Discharges reported at the two USGS gages seem to have a positive relationship (Figure 8). However, records of discharge at the downstream Wallisville gage, indicated the maximum inflow at that site does not exceed 23,000 cfs regardless the discharge recorded at the upstream Romayor gage. This indicates that some river discharge is diverted before reaching the Wallisville gage.

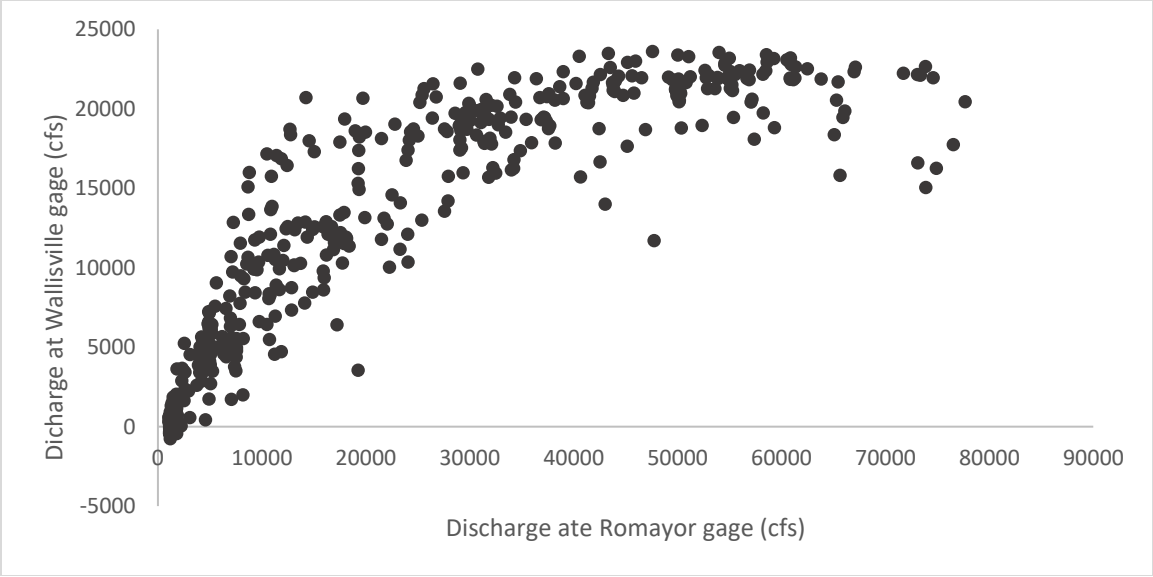

Figure 8. Discharge records at USGS gages at Romayor and Wallisville for the study period.

The salinity at local sites exhibited differing degrees of correlation with the discharge recorded at the Romayor and Wallisville gages. In general, sites local salinity tend to be more correlated to (affected by) freshwater inflow amount at Wallisville (Table 4).

Table 4. Correlation between salinity measured at each local site and freshwater inflow measured at the Romayor and Wallisville gages.

Site	Wallisville discharge		Romayor discharge	
	Correlation coefficient	**p-value**	**Correlation coefficient**	**p-value**
R38	-0.63	<0.0001	0.01	<0.0001
R13	-0.60	<0.0001	0.34	<0.0001
T7	-0.54	<0.0001	-0.11	<0.0001
T3	-0.52	<0.0001	0.06	<0.0001
R31	-0.59	<0.0001	0.14	<0.0001
T6	-0.65	<0.0001	-0.13	<0.0001
R49	-0.40	<0.0001	0.28	<0.0001
R48	-0.29	<0.0001	0.02	<0.0001
R18	-0.07	0.0008	0.09	0.1634
R45	0.56	<0.0001	0.83	<0.0001

Water temperature variation by site

The average temperature for all study sites ranged from 22.4 °C at site T6 to 23.9 °C at site T3 where the highest single temperature 33.8 °C was recorded. The lowest temperatures, 6.4 °C and 5.2 °C, were recorded at sites R31 and T7 respectively (Table 5). Nonparametric tests, Kruskal–Wallis and Mann-Whitney pairwise, were used to detect and measure variance in median temperature between sites (Figure 9).

Table 5. Summary table of temperature and water depth.

Site	Temperature				Average Depth (m)
	Maximum	Average	Median	Minimum	
R38	32.0	22.6	23.5	10.8	0.74
R13	31.9	22.9	22.1	8.2	0.81
T7	33.6	22.6	23.7	5.2	0.45
T3	33.8	23.9	22.6	9.4	0.65
R31	33.2	23.0	23.8	6.4	0.54
T6	32.1	22.4	24.6	7.8	0.66
R49	32.5	23.7	25.3	10.4	0.65
R48	32.3	23.2	23.2	9.9	0.40
R18	32.4	22.4	22.9	10.8	0.67
R45	32.6	23.8	25.5	10.3	0.27

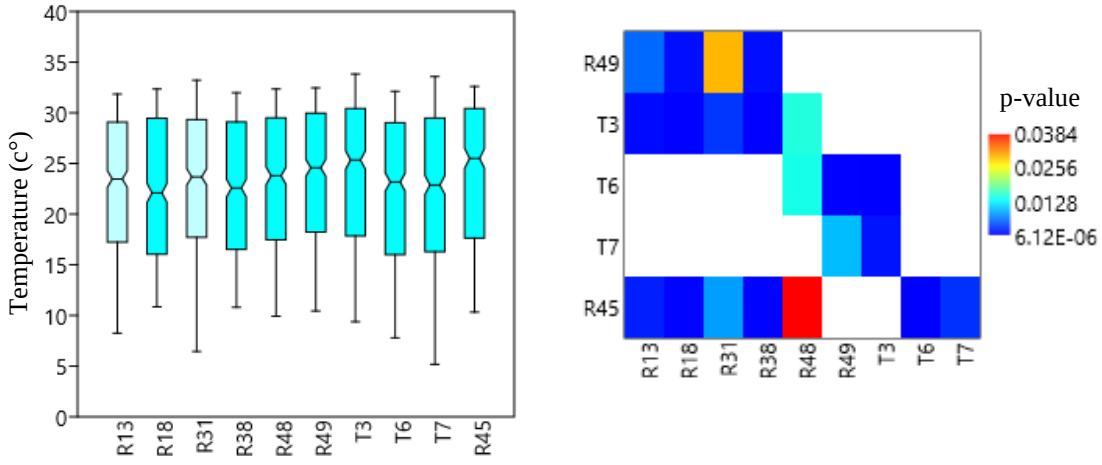

Figure 9. Variation in temperature between sites. A) Boxplot of median temperature by site (notches show 95% confidence interval). B) Matrix plot depicting significant differences (p-value < 0.05) in temperature between sites.

Sediment type and fine percent

On the quarterly temporal scale, samples collected in July and April 2018 had the highest average percent fines (61.4 and 59.1%, respectively) while the lowest average percent fines (34.9%) were measured from samples collected in January 2019 (Table 6). Nonsignificant ($p>0.05$) negative correlations were observed between the average percent fines per sampling event and the historical freshwater inflow based on the last 60 and 90 days of discharge measured at the Romayor ($r = -0.71$ and -0.69, respectively) and Wallisville ($r = -0.69$ and -0.73, respectively) gages.

On the spatial scale, the average percent fines was the highest (62.8%) at site R18 in contrast to site T7 where the average percent fines was the lowest (38.2%). All sites exhibited various degrees of negative correlation between average percent fines and freshwater inflow, except for R38 where average percent fines was positively correlated with inflow. However, only 3 sites (R13, R18 and R45) showed statistically significant negative correlations between average percent fines and historical freshwater inflow measured as average discharge at Romayor and Wallisville for the preceding 90 days (average discharge for preceding 60 and 30 days did not show clear correlation pattern) (Figure 10).

Table 6. Summary table of sediment percent fines for all sites from each sampling event during the study period.

Site	Sediment sampling event					Average Fine % per site
	Apr-18	Jul-18	Jan-19	Apr-19	Jul-19	
R13	52.7	72.7	21.3	53.3	46.0	49.2
R18	70.3	77.7	42.0	65.3	58.7	62.8
R31	60.7	56.7	14.0	63.3	73.3	53.6
R38	71.3	30.7	60.7	56.7	62.7	56.4
R45	48.7	67.0	12.0	45.3	38.0	42.2
R48	56.3	84.7	60.0	50.7	56.0	61.5
R49	64.7	49.0	36.7	17.3	61.3	45.8
T3	28.0	63.7	55.3	24.7	54.7	45.3
T6	76.0	36.3	28.0	29.3	52.0	44.3
T7	62.0	75.3	18.7	14.7	20.7	38.3
Average fines % per sampling event	59.1	61.4	34.9	42.1	52.3	

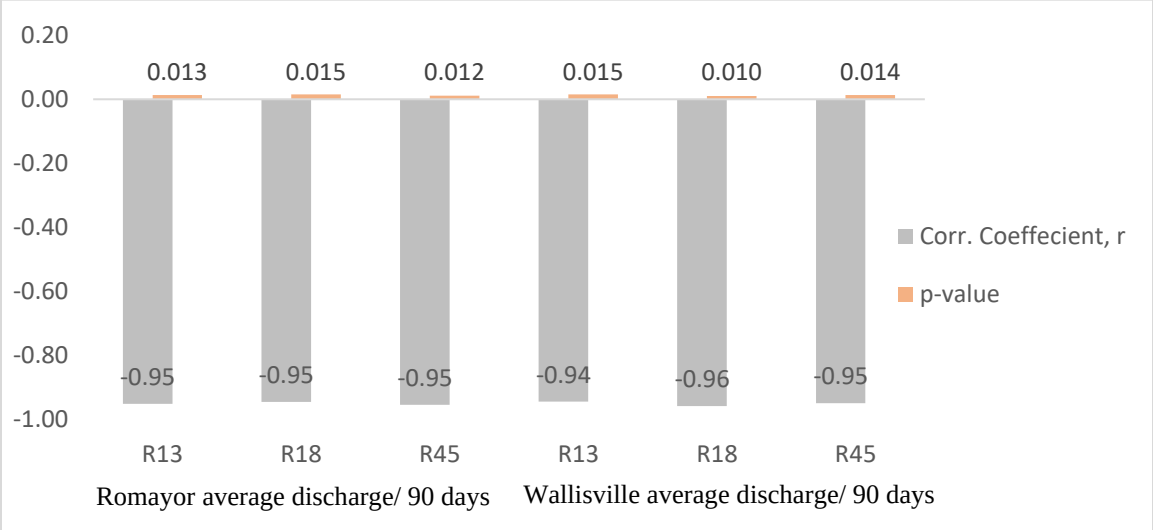

Figure 10. Significant correlation coefficient and p-values observed between average percent fines and historical freshwater inflow. Average discharge/90 days = the average of all discharge records for the last 90 days prior collecting sediment samples.

Other environmental parameters were measured on sampling events including dissolved oxygen (DO mg/L), Secchi tube for clarity (m) and pH. Nonparametric tests, Kruskal–Wallis and Mann-Whitney pairwise, were used to detect and measure variance in median DO and Secchi depth per sampling event (Figure 11). Median dissolved oxygen varied slightly between sites where sites R13 and T3 recorded the highest average dissolved oxygen while Site R18 recorded the lowest average dissolved oxygen (Table 7). Median dissolved oxygen varied among sampling events (Figure 11) where the median dissolved oxygen for January and April 2019 were significantly higher than other sampling events. Recorded pH and Secchi tube for the study are listed in Table 8).

Table 7. Summary table of dissolved oxygen (mg/L), DO, throughout the study.

Site		**Apr-18**	**Jul-18**	**Jan-19**	**Apr-19**	**Jul-19**	**Average per site**
R13	Surface	7.06	9.49	10.33	10.57	7.77	9.03
	Bottom	7.05	9.24	10.29	10.53	7.96	
R18	Surface	6.93	5.79	10.26	9.1	6.72	7.74
	Bottom	6.96	5.64	10.26	9.08	6.68	
R31	Surface	10.23	9.61	9.91	9.62	8.2	8.99
	Bottom	10.23	9.61	9.52	9.42	3.5	
R38	Surface	7.01	6.24	10.19	9.43	7.41	8.01
	Bottom	7	6.15	10.18	9.34	7.15	
R45	Surface	6.93	8.26	10.32	9.21	8.55	8.64
	Bottom	6.97	8.22	10.3	9.24	8.38	
R48	Surface	7.07	5.59	10.32	9.17	7.27	7.86
	Bottom	7.09	5.49	10.31	9.16	7.17	
R49	Surface	7.44	8.75	9.93	9.52	7.81	8.65
	Bottom	7.56	8.32	9.89	9.48	7.78	
T3	Surface	7.3	8.66	10.49	10.13	8.67	9.02
	Bottom	7.28	8.53	10.49	10.11	8.57	
T6	Surface	7.09	5.9	10.34	9.27	6.97	7.91
	Bottom	7.03	5.91	10.33	9.26	6.95	
T7	Surface	7	9.27	10.26	10.1	8.67	8.97
	Bottom	6.98	9.27	10.26	10.1	7.78	
Average per event		7.41	7.70	10.210	9.59	7.50	

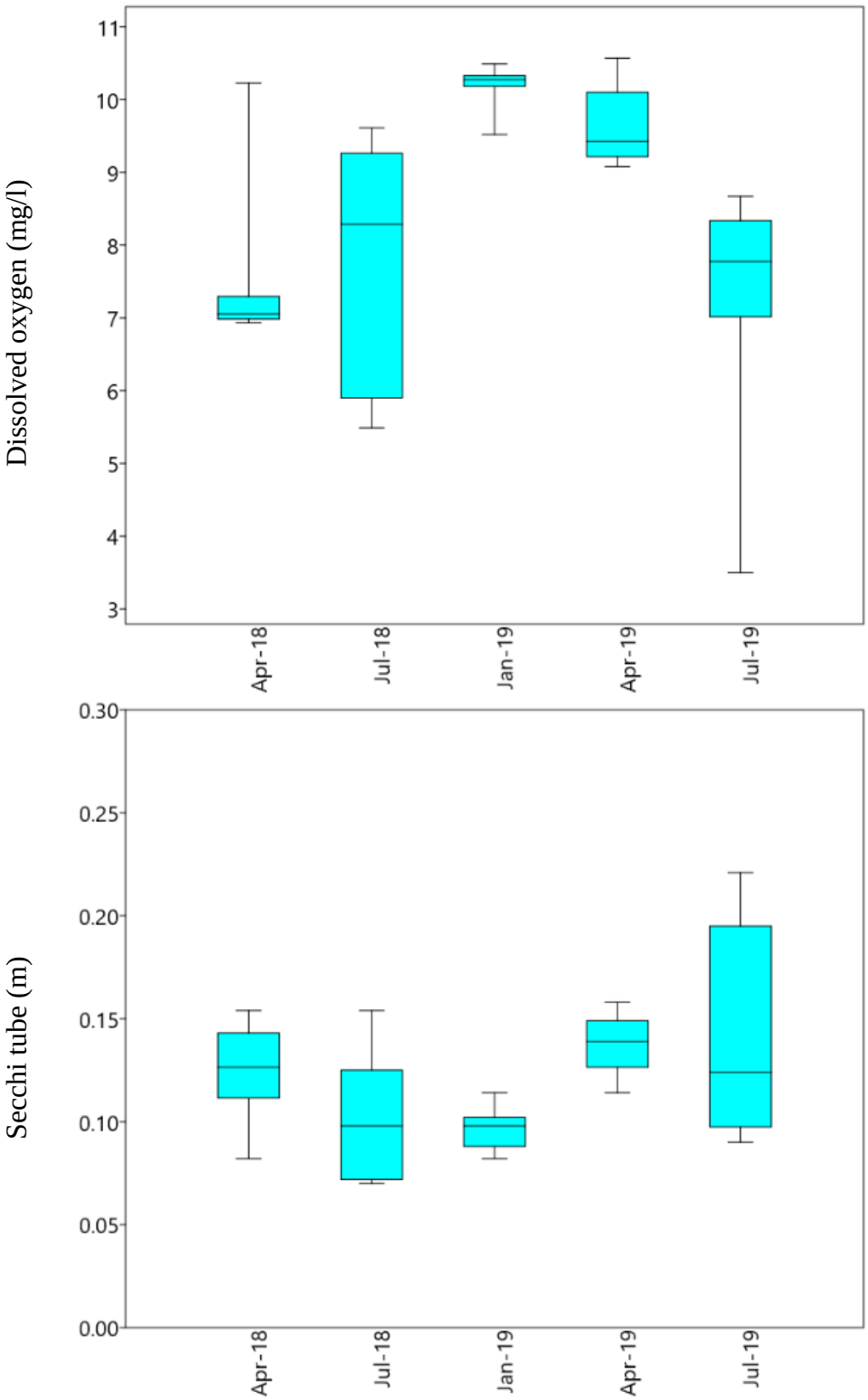

Figure 11. Boxplot of variation in dissolved oxygen per sampling event (upper panel) and water clarity as measured with a Secchi tube (lower panel).

Table 8. Summary of Secchi tube and pH records for each site collected during all sampling events.

Site	Secchi (m)					Site Average	pH					Site Average
	Apr-18	Jul-18	Jan-19	Apr-19	Jul-19		Apr-18	Jul-18	Jan-19	Apr-19	Jul-19	
R13	0.140	0.140	0.088	0.152	0.132	0.130	7.50	8.67	7.57	8.42	8.09	8.05
R18	0.122	0.154	0.098	0.144	0.221	0.148	7.50	8.12	7.57	7.92	7.75	7.77
R31	0.092	0.072	0.082	0.122	0.120	0.098	8.05	8.99	7.72	8.17	8.02	8.19
R38	0.152	0.120	0.098	0.133	0.190	0.139	7.42	7.81	7.44	8.00	8.18	7.77
R45	0.129	0.100	0.090	0.158	0.090	0.113	7.49	8.40	7.55	7.95	8.00	7.88
R48	0.124	0.120	0.100	0.148	0.210	0.140	7.50	7.75	7.52	7.95	7.94	7.73
R49	0.154	0.070	0.108	0.128	0.116	0.115	7.52	8.61	7.59	8.08	7.83	7.92
T3	0.082	0.072	0.088	0.138	0.090	0.094	7.54	8.48	7.63	8.19	8.22	8.01
T6	0.134	0.080	0.100	0.140	0.100	0.111	7.50	8.19	7.56	7.96	8.02	7.84
T7	0.118	0.096	0.114	0.114	0.128	0.114	7.48	8.86	7.59	8.20	7.92	8.01
Average	0.124	0.102	0.096	0.137	0.139		7.54	8.37	7.52	8.08	7.99	

Rangia cuneata population dynamics

Abundance

Rangia cuneata collected during the November 2018 sampling event and any opportunistic clams collected throughout the study were excluded from spatiotemporal analysis of abundance data. In total, 337 *R. cuneata* were included in abundance calculations. Ratios of live to dead but whole and hand to rake sampled among total collected clams are summarized in Table 9).

Table 9. Number of *R. cuneata* collected by live/dead status and sampling method.

Live or dead	Method		Total
	Hand sampled	Rake sampled	
Live	201	47	248
Dead (but whole)	71	18	89
Total	272	65	337

Total catch per site

Total cumulative abundance of *R. cuneata* per site (total catch collected by the two sampling methods, hand and rake sampling, summed over all sampling events) varied greatly (Figure 12). Highest total abundance occurred at sites R49, R48, R38 and R13. In contrast, the lowest total catch of *R. cuneata* occurred at sites R45 and R18 (Figure 12).

Among all sites, R48 showed the highest abundance of live *R. cuneata* with no single dead clam collected on all sampling events (total 109 *R. cuneata* collected by hand sampling, rake sampling and opportunistic). In contrast, a high percentage of *R. cuneata* collected from site R49 were dead but whole (out of a total 126 *R. cuneata* collected by hand sampling, rake sampling and opportunistic; 51 of them were dead).

Sites with relatively high total cumulative abundance (R49, R48, R38 and R13) also produced consistent catches of *R. cuneata* during all sampling events. On the other hand, low total cumulative abundance in other sites (R18, R45, T6, T7, T3 and R31) was a result of inconsistently catching a few numbers of clams on some sampling events (Figure 13).

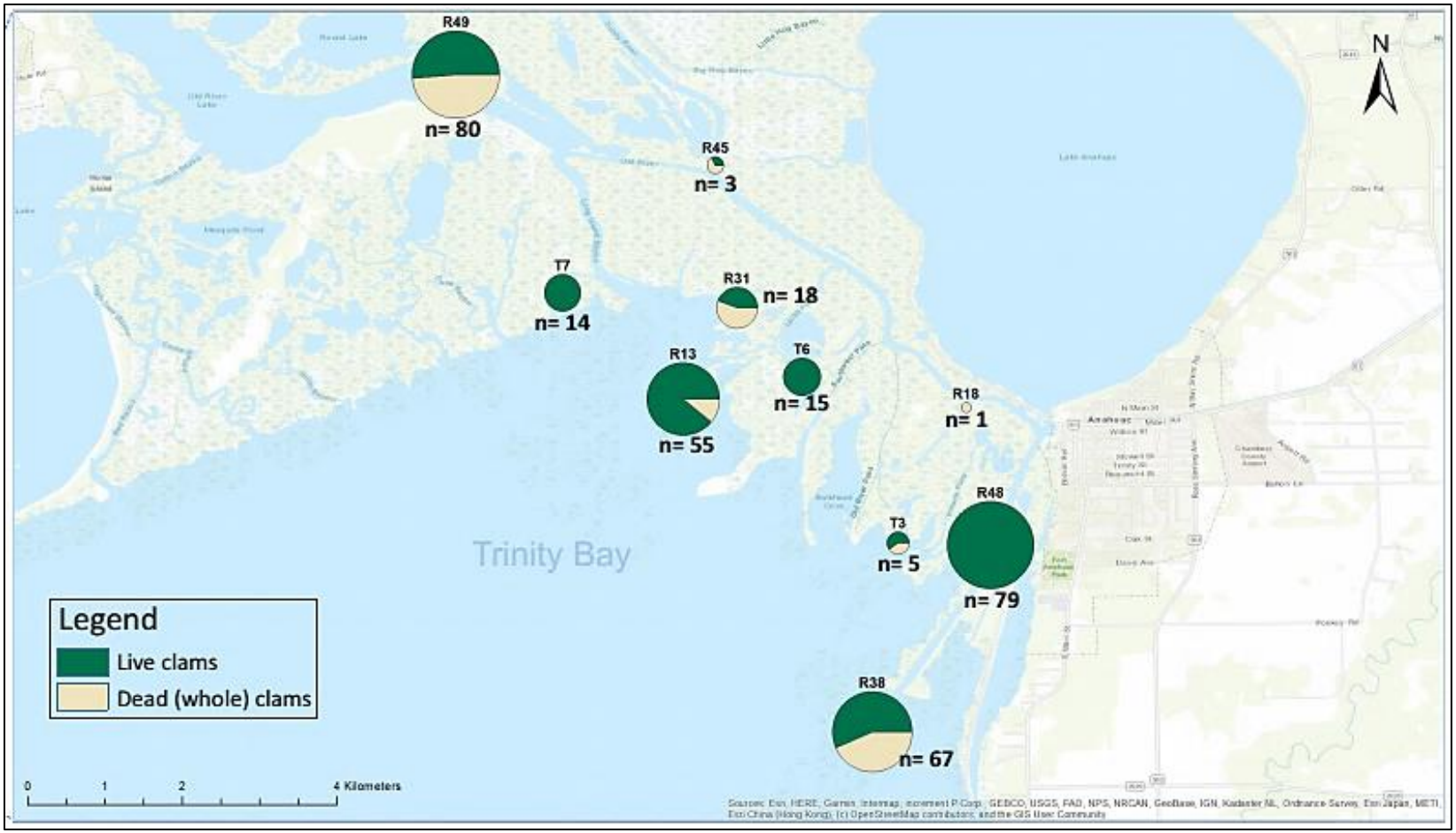

Figure 12. Total Abundance of *R. cuneata* in different study sites. Proportional pie graphs depicting the % composition of the total catch (live and recently dead but whole) clams collected from each site using the two standardized methods, hand and rake sampling.

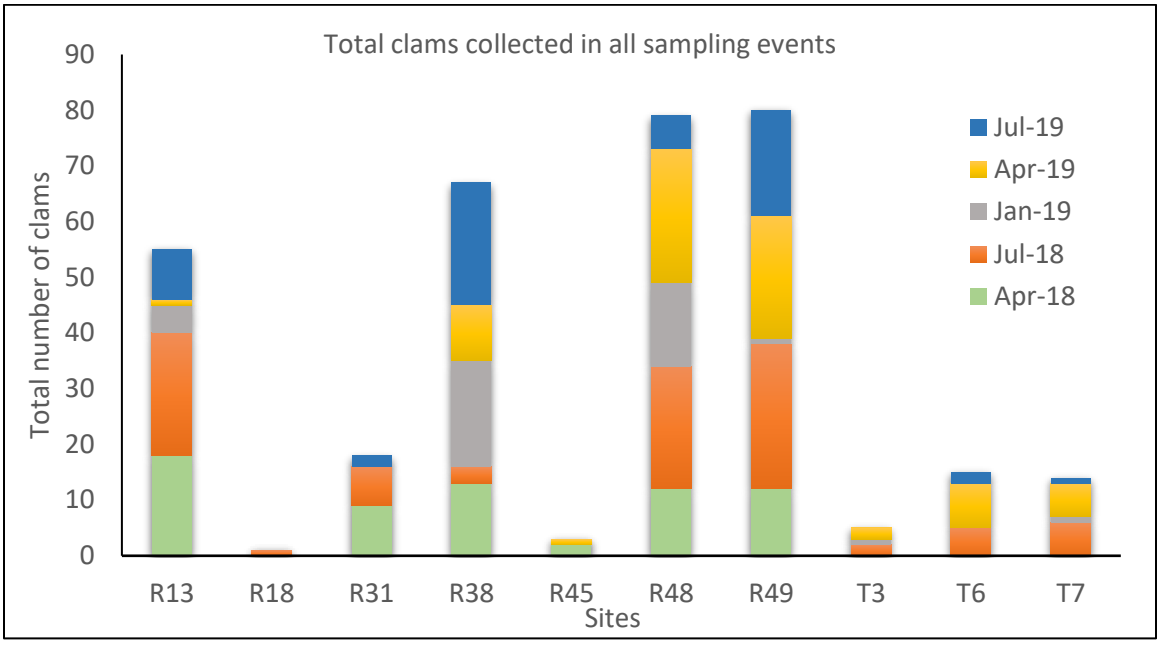

Figure 13. Rangia cuneata catch by site by sampling event.

Catch per unit effort (CPUE)

Rangia cuneata were collected by hand sampling an area of 3 m^2 (3 quadrats, 1 m^2 each) plus rake sampling (3 rake drags, 30 seconds each). This same level of effort was implemented at each site per event. Therefore, CPUE values presented herein are for each site on each sampling event and include the total *R. cuneata* caught with all replicates of both hand sampling and rake sampling combined (Table 10).

Total catch per sampling event from all sites (by hand and rake methods) is shown in Table 10). The reported CPUE of *R. cuneata* was recorded to be higher in July (average July catch) than April (average April catch) while CPUE in January was the lowest.

Table 10. Summary of catch and catch per unit effort (CPUE) by site and sampling event. CPUE for each collection (site x date) based on 6 replicate units of effort.

Site	Apr-18		Jul-18		Jan-19		Apr-19		Jul-19		Site Avg
	Catch	CPUE	Catch	CPUE	Catch	CPUE	Catch	CPUE	Catch	CPUE	CPUE
R13	18	3.00	22	3.67	5	0.83	1	0.17	9	1.50	1.83
R18	0	0.00	1	0.17	0	0.00	0	0.00	0	0.00	0.03
R31	9	1.50	7	1.17	0	0.00	0	0.00	2	0.33	0.60
R38	13	2.17	3	0.50	19	3.17	10	1.67	22	3.67	2.23
R45	2	0.33	0	0.00	0	0.00	1	0.17	0	0.00	0.10
R48	12	2.00	22	3.67	15	2.50	24	4.00	6	1.00	2.63
R49	12	2.00	26	4.33	1	0.17	22	3.67	19	3.17	2.67
T3	0	0.00	2	0.33	1	0.17	2	0.33	0	0.00	0.17
T6	0	0.00	5	0.83	0	0.00	8	1.33	2	0.33	0.50
T7	0	0.00	6	1.00	1	0.17	6	1.00	1	0.17	0.47
Event Avg CPUE		1.10		1.57		0.70		1.23		1.02	
Event Total catch	66		94		42		74		61		

Morphometrics and size distribution

A total of 559 *R. cuneata* individuals (live, n = 490, and dead, n = 109) were collected across the study period from all sites using all used methods (hand, rake and opportunistic sampling). Morphometrics measurements on clams included length, height and width. Additionally, shells from 330 live clams were weighed as part of the MI calculation protocol.

The average length of all collected *R. cuneata* (live and dead) was 56.7 mm with a range of 10.5 mm up to 80.1 mm. Live and dead *R. cuneata* showed different length ranges and average lengths (Table 11). Live clam recorded average length of 56.24 mm with a minimum and maximum length 10.5 mm and 78.6 mm, respectively. Dead *R. cuneata* length ranged from 34.3 mm to 80.1 mm with an average length 58.2 mm. The average height of all *R. cuneata* (live and dead) was 36.4 mm and the average width was 49.6 mm.

Table 11. Summary table of shell size (length) for different groups of collected *R. cuneata*.

Clam group	**Length**			**Width**			**Height**		
	Max.	**Average**	**Min**	**Max.**	**Average**	**Min**	**Max.**	**Average**	**Min**
All *R. cuneata*	80.1	56.7	10.5	57.8	36.4	4.5	72.9	49.6	7.9
Live	78.6	56.2	10.5	57.8	36.1	4.5	69.3	49.3	7.9
Dead	80.1	58.7	34.3	53.4	37.8	21.8	72.9	51.4	30.3

Spatiotemporal distribution of shell size

Spatiotemporal variation in shell size was measured using nonparametric tests: Kruskal–Wallis and Mann-Whitney pairwise. On the spatial scale, shell size (represented by length) distribution varied between sites where sites R49 and R31 had significantly higher average shell length from all other sites in contrast to site T7 which was significantly lower in average length than all sites (except R45 and R18). Only 16 (out of 559 total) juvenile *R. cuneata* were collected during the study from only 6 sites (T7 = 4, R13 = 4, T6 = 3, R49 = 2, R31 = 2 and R18 = 1) (Figure 14).

On the temporal scale, little difference was observed between sampling events except November 2018 and January 2019 when shell length showed slightly lower (but statistically significant) average compared to July 2019 (Figure 15).

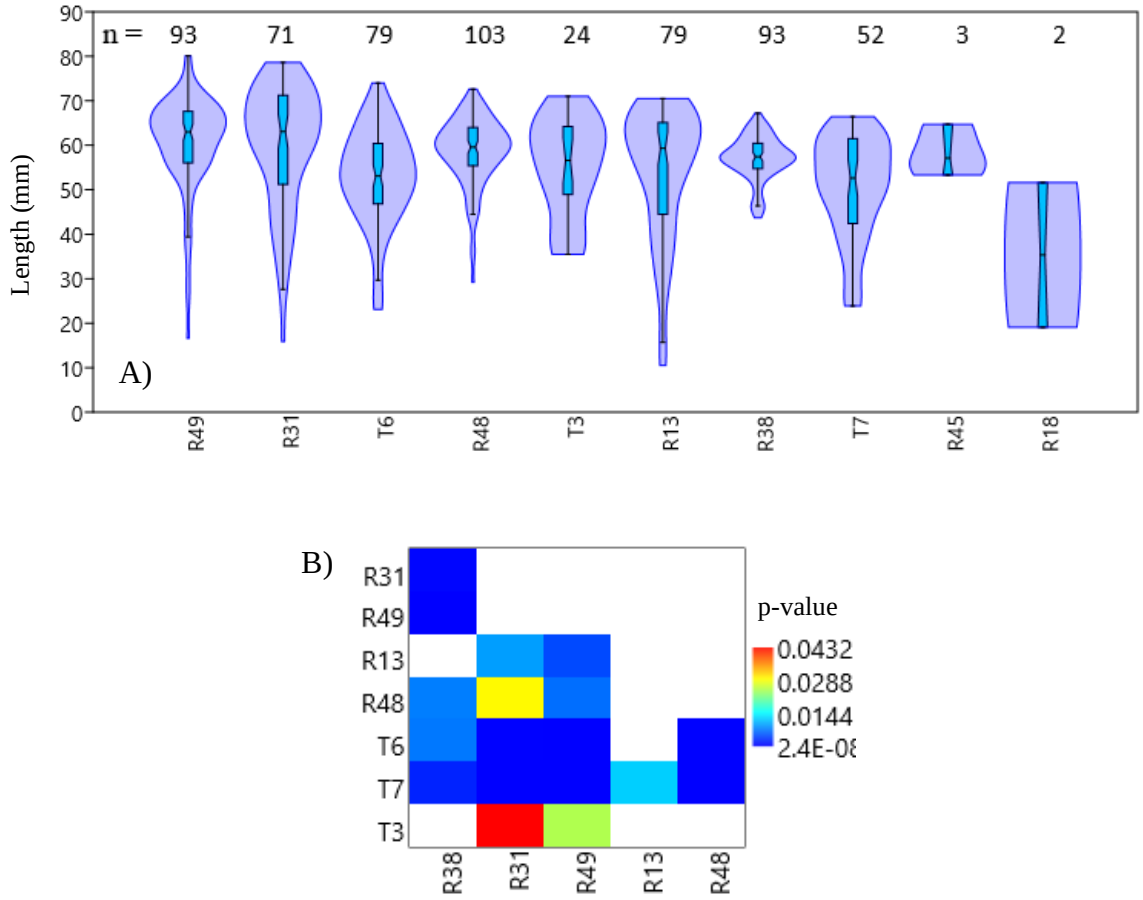

Figure 14. Spatial variation in *R. cuneata* catch throughout the study. A) Violin and boxplot for shell size distribution per sites. B) Matrix plot shows the significantly different sites represented by p-value < 0.05 (paired sampling events that did not exhibit statistical significance are not plotted).

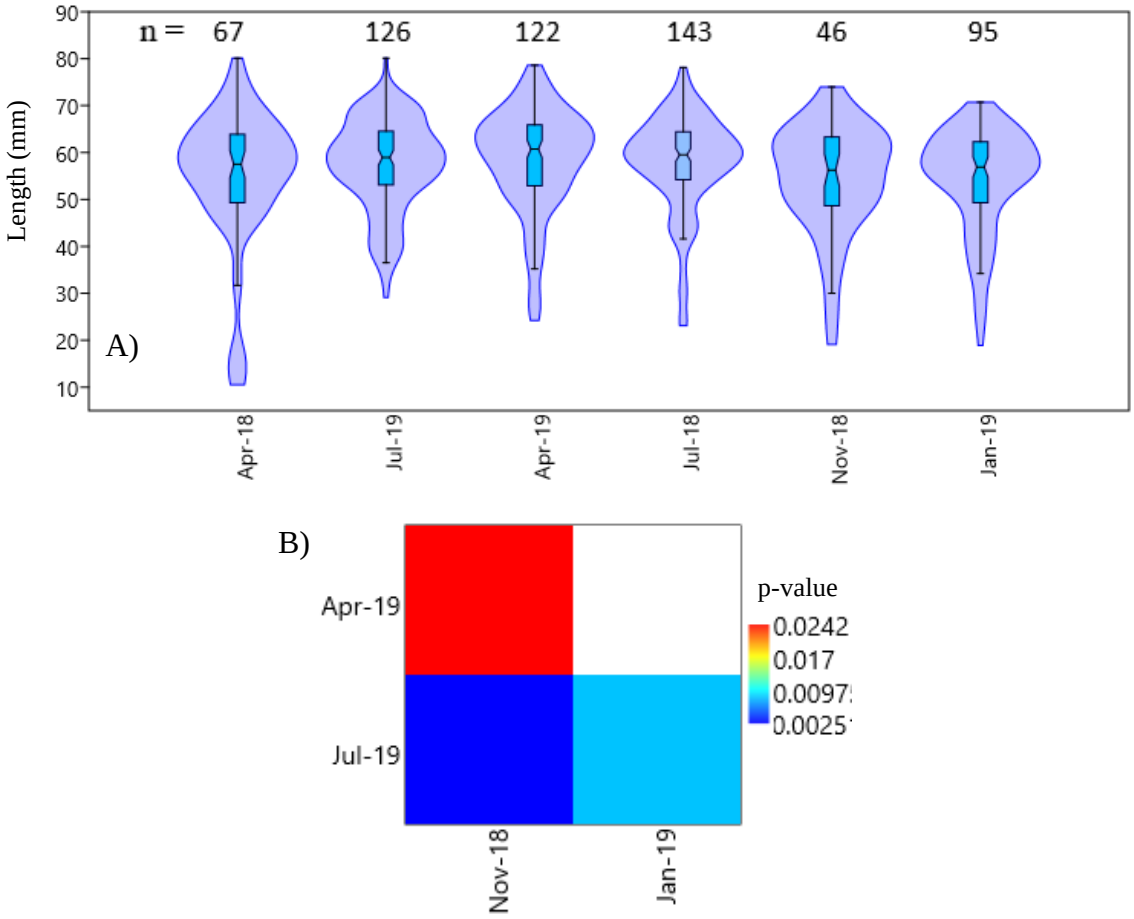

Figure 15. Temporal variation in *R. cuneata* catch throughout the study. A) Violin and boxplot for shell size distribution per sampling event. B) Matrix plot shows the significantly different sampling events represented by p-value < 0.05 (paired sampling events that did not exhibit statistical significance are not plotted).

Meat Index as health indicator

Meat index was measured for up to 10 *R. cuneata* per site per sampling event. Two sites, R18 and R45, were excluded from further MI analysis since only one clam from each site was measured for MI throughout the study. Total *R. cuneata* whose MI was measured from all sites on all sampling events added up to 316 *R. cuneata* (Juvenile (n=12) and adult *R. cuneata*(n=304). Average MI for this study was 22 ranging from 10.85 to 58.84.

Meat index in relation to size (length)

Meat index seems to be affected by the size (age) of the clam, e.g. juvenile *R. cuneata* (< 28 mm, according to Windham (2015)) tend to accumulate more meat than older ones. Figure 16) shows the relationship between the individual clam length and their MI.

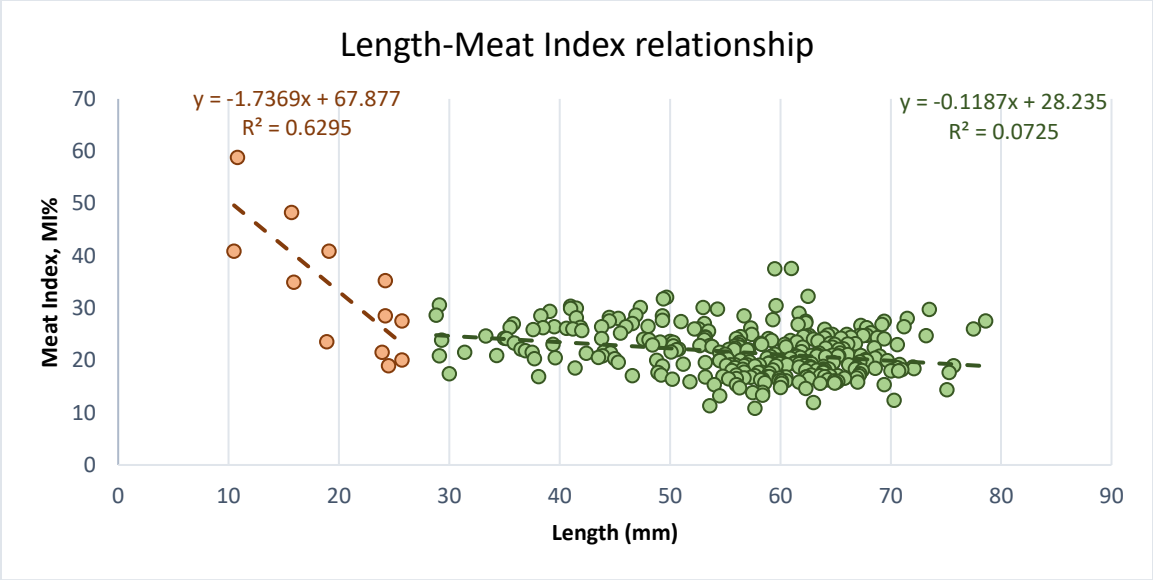

Figure 16. Relationship between MI and shell length in juvenile (orange) and adult (green) *R. cuneata*.

Spatiotemporal variation in MI

Only adult *R. cuneata* MI data were measured for spatiotemporal variation. On the temporal scale, results from Kruskal-Wallis and Mann-Whitney tests showed significant difference between MI collected during different sampling events. April 2018 sampling event showed significantly lower MI than all other sampling events (Figure 17).

On the spatial level, results from Kruskal-Wallis and Mann-Whitney tests showed significant difference between overall median MI per site (median MI collected at the same site throughout the study period). Median MI of *R. cuneata* collected from site R38 (exposed to highest salinity) throughout the study was significantly lower than other sites. Also, sites T7 and T6 showed significantly higher median MI than site R49 (Figure 17).

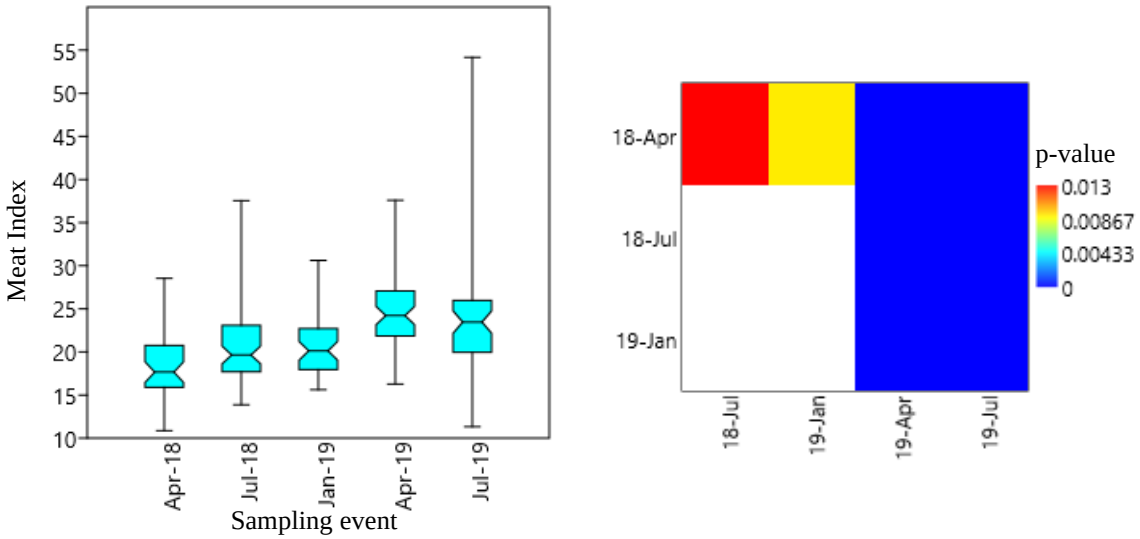

A) Temporal variation in MI

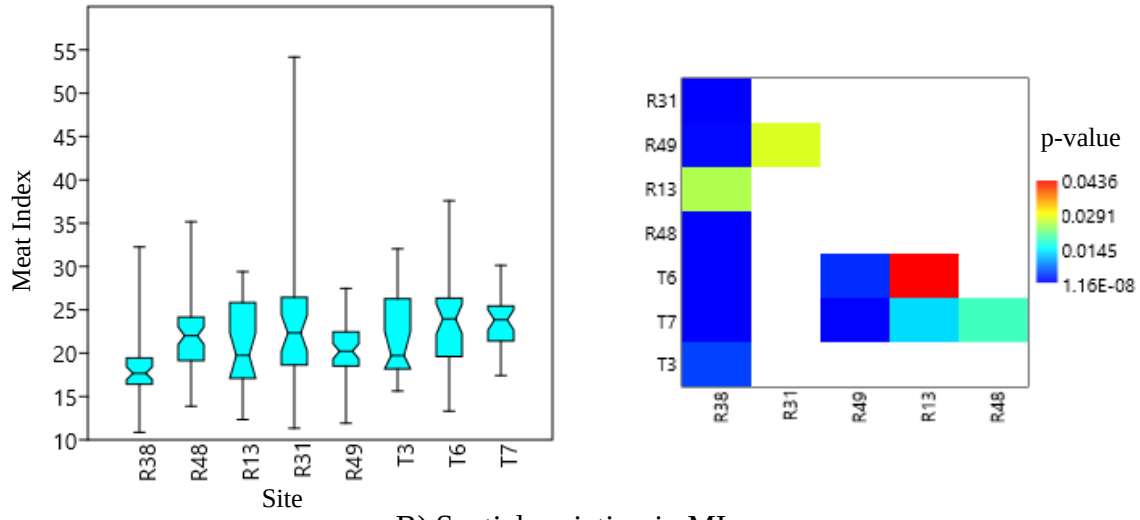

B) Spatial variation in MI

Figure 17. Spatiotemporal variation in MI as depicted by boxplots. A) Temporal variation in MI: Median MI per sampling event (left panel) and matrix plot of significance (p-value, right panel). B) Spatial variation in MI: Median MI per site (left panel) and matrix plot of significance (p-value, right panel).

Influence of environmental variables on MI

To evaluate the potential impact of associated environmental conditions (salinity, temperature, percent fines and Secchi tube) on MI, a correlation-based Principal Component Analysis (PCA) test was used to determine which environmental factors correlated with MI (Figure 18).

The PCA loading graph, average daily salinity magnitude (DSM) for the last 30, 60 and 90 days showed negative correlation with MI (Figure 18). By testing correlation between MI and each environmental variable separately, only daily salinity magnitude for the last 90 and 60 days and sediment percent fines show significant moderate negative correlation with MI (Figure 19).

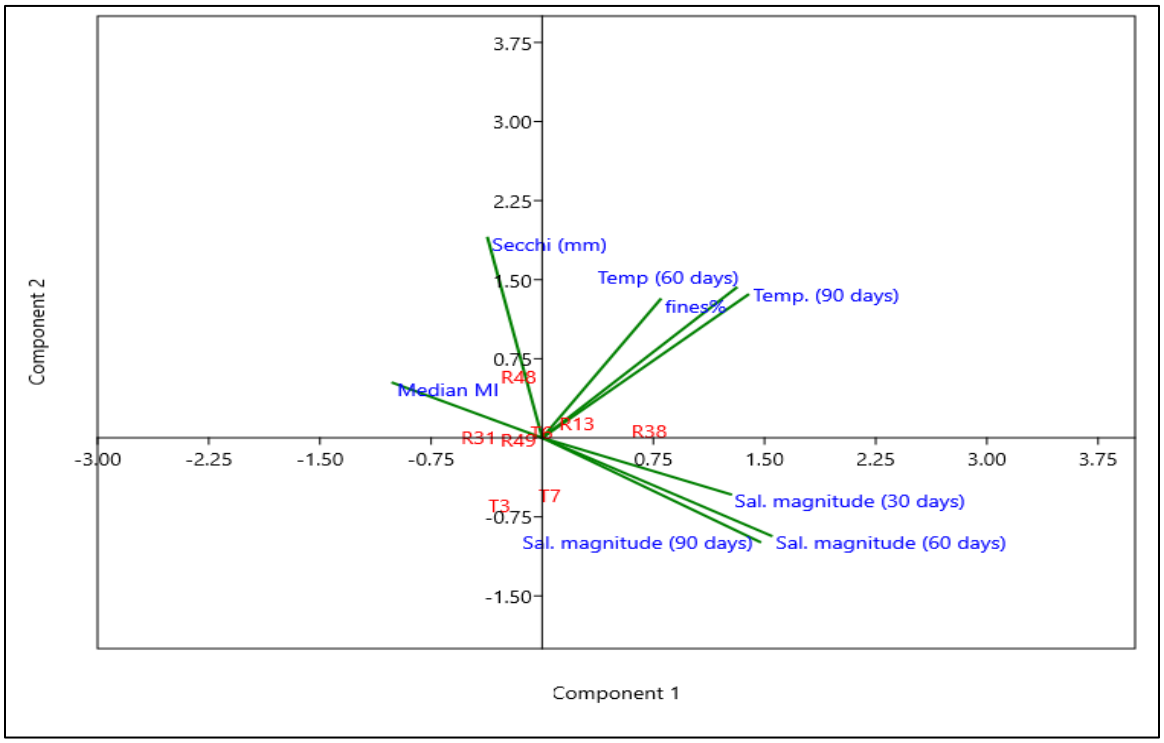

Figure 18. Principal Components Analysis loading plot shows relationship between environmental variables, MI and principal components. Median MI = median meat index. Temp = Temperature. Sal. magnitude = Average daily salinity magnitude. Secchi (mm) = Secchi tube reading.

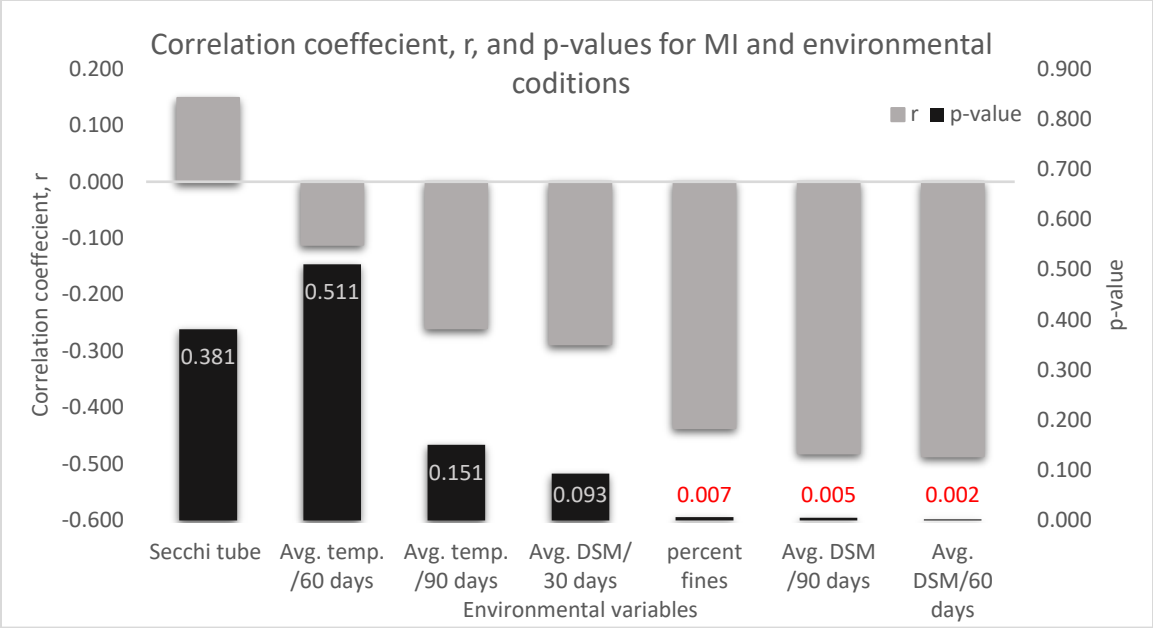

Figure 19. Correlation coefficient (r), and p-value for relationship between meat index (MI) and environmental variables. Avg. DSM = Average daily salinity magnitude. Avg. temp = Average temperature.

Effect of salinity on MI

Rangia cuneata seemed to have different growth variables (e.g. abundance and average shell length) per different sites due to variation in environmental conditions among sites. This variation suggested that the average response whole *R. cuneata* population TRD to a given environmental variable did not necessarily reflects the response of subpopulations (*R. cuneata* at different sites). To improve the understanding of the relationship between MI and the environmental variables, MI data was analyzed on two levels, population and subpopulations levels. Population levels refers to all sites combined, and subpopulations level refers to each site separately.

To measure the potential impact of varying inflow and resulting salinity on the MI at the population level, median MI from each site during each sampling event were tested for correlation with average preceding inflow and average daily salinity magnitude for

the preceding 30, 60 and 90 days. Freshwater inflow data from USGS gages at Trinity River at Wallisville and Romayor were utilized for this analysis. The median MI exhibited significant negative correlations with average DSM for the last 90 (r = -0.48, p= 0.005) and 60 days (r = -0.48, p= 0.005) (Figure 20). None of the other inflow or salinity variables exhibited significant correlations with the MI.

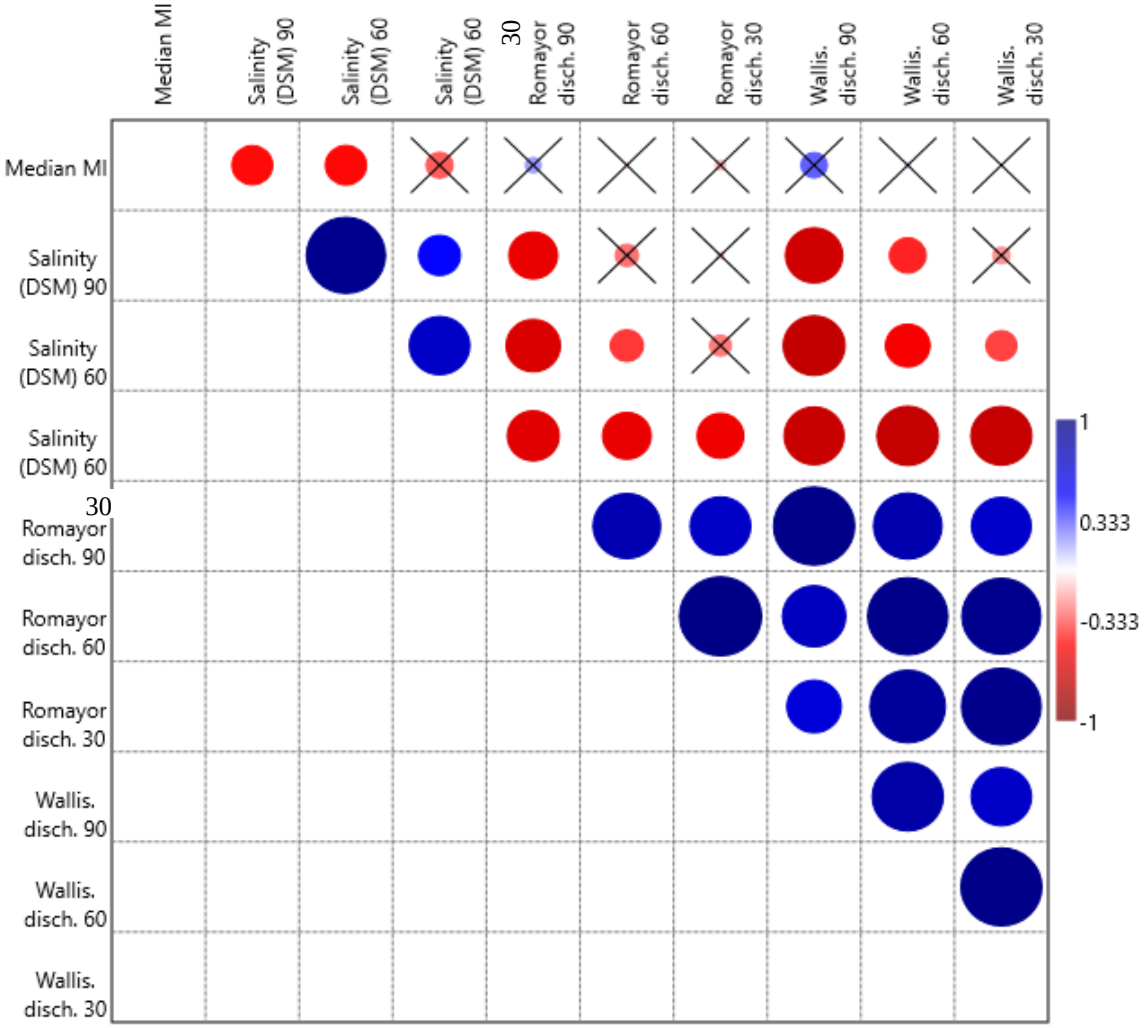

Figure 20. Multiple correlation plot shows MI correlation with salinity and inflow variables. Color shows direction of correlation (Blue for positive, and red for negative correlation). Color intensity indicates strength of correlation. Crossed circles show insignificant ($p > 0.05$) correlation. Median MI = median meat index. Salinity (DSM)/ (n) = Average daily salinity magnitude for n number of days (30, 60 or 90). Romayor or Wallis. disch. (n) = average of historical discharge (inflow) from Romayor or Wallisville gage for n number of days (30, 60 or 90).

To measure the potential effect of varying inflow and resulting salinity on the MI at the sub-population level, the median MI from each site was tested for correlation with average DSM for the preceding 90 and 60 days. The median MI from different sites exhibited degrees of correlations with associated local site salinity. Only sites R13 and R31 showed significant negative correlations with average DSM for the preceding 90 and 60 days. None of the other sites showed any significant correlation with average DSM. All sites showed nonsignificant correlation with freshwater inflows at Romayor and Wallisville. However, some of these sites (R13 and R31) exhibited strong (nonsignificant) correlations between median MI and the average freshwater inflow for the last 90 and 60 days.

Effect of sediment percent fines on MI

At the subpopulation level, no significant correlation was measured between MI and percent fines of the sediment at any of the study sites although at some sites (R49, R13 and T3) the MI exhibited strong ($r = -0.71$ to -0.89) but not significant correlation with percent fines in sediment.

Temporal variation in MI in response to environmental variables

Median MI of all *R. cuneata* collected on a given sampling event was not significantly correlated with average freshwater inflow (at Romayor and Wallisville) or average daily water temperature for the last 90, 60 or 30 days. Sediment fines percent exhibited a weak nonsignificant correlation with the MI collected per sampling event.

Combined effect of environmental variables on MI (Multiple regression analysis)

The combined effect of salinity, sediment percent fines and temperature on MI were tested by running a multiple regression analysis. Results show that models that include multiple variables explain more of the variation in MI (higher r^2 and adjusted r^2) than simpler models consisting of just one explanatory variable (Table 12).

Table 12. R square (R^2), adjusted $R^2$and p-values for multiple regression between MI and combinations of environmental variables. Parameters of linear model = a, b, c, d. DSM/60 days = Average daily salinity magnitude for the last 60 days. Fines% = Sediment percent fines. Temperature (60 days) = Average temperature for the last 60 days.

Linear Regression Model and Variables Tested	**R^2**	**Adjusted R^2**	**p-value**
MI = a + b (DSM/ 60 days)	0.236	0.215	0.002
MI = a + b (DSM/ 60 days) + c(fines%)	0.281	0.238	0.003
MI = a + b (DSM/ 60 days) + c(fines%) + d (Temperature (60 days))	0.401	0.347	0.001

Shell structure and age

Shell dimensions and weight

Regression analysis between shell dimensions (L, W, H and TD) shows that TD was more correlated with each L, W and H than these shell variables were correlated to each other (Figure 21). This indicates that total dimensions (TD) captures and accurately represents the various dimensions of a shell size better than any single dimension.

During *R. cuneata* laboratory examination, some shells were observed to be longer than other shells for the same width, height or shell weight range. We therefore calculated multiple ratios of shell dimensions including Length: Height ratio and Length: Width ratio as markers of shell elongation. Kruskal–Wallis test and Mann-Whitney

pairwise tests were used to determine if any significant difference in these ratios between sites (Figure 22). Two sites (R45 and R18) were excluded from further data analysis due to limited catch throughout the study (2 *R. cuneata* individuals from R18 and 3 from R45, remaining n = 594). Results show that site T6 had a significantly larger length: height and length: width ratios than all other sites except site T7 (Figure 22).

The ratio between total dimensions (TD) and shell weight was evaluated. This ratio is a function of how thick the valve of the shell is. When *R. cuneata* are stressed, they may not invest resources into shell deposition at the rate that they do when they are otherwise healthy. I recommend this ratio as an indicator of health and will henceforth be referred to as "shell index", calculated as following:

$$\text{Shell index} = \frac{\text{Empty shell weight}}{\text{Total shell dimensions (TD)}}$$

Rangia cuneata collected from sites T6 and T7 had significantly lower shell index than *R. cuneata* from other sites (except from site R13) (Figure 22). To avoid the effect of shell size on the shell index comparison among sites, shell index for was compared among sites for the same age (based on age data from individuals previously aged during this study). Differences in shell index at the same age were noticed among sites. *Rangia cuneata* individuals collected from sites R49 and R48 had higher shell index than individuals from sites T6 and T7 for the same age (Figure 23).

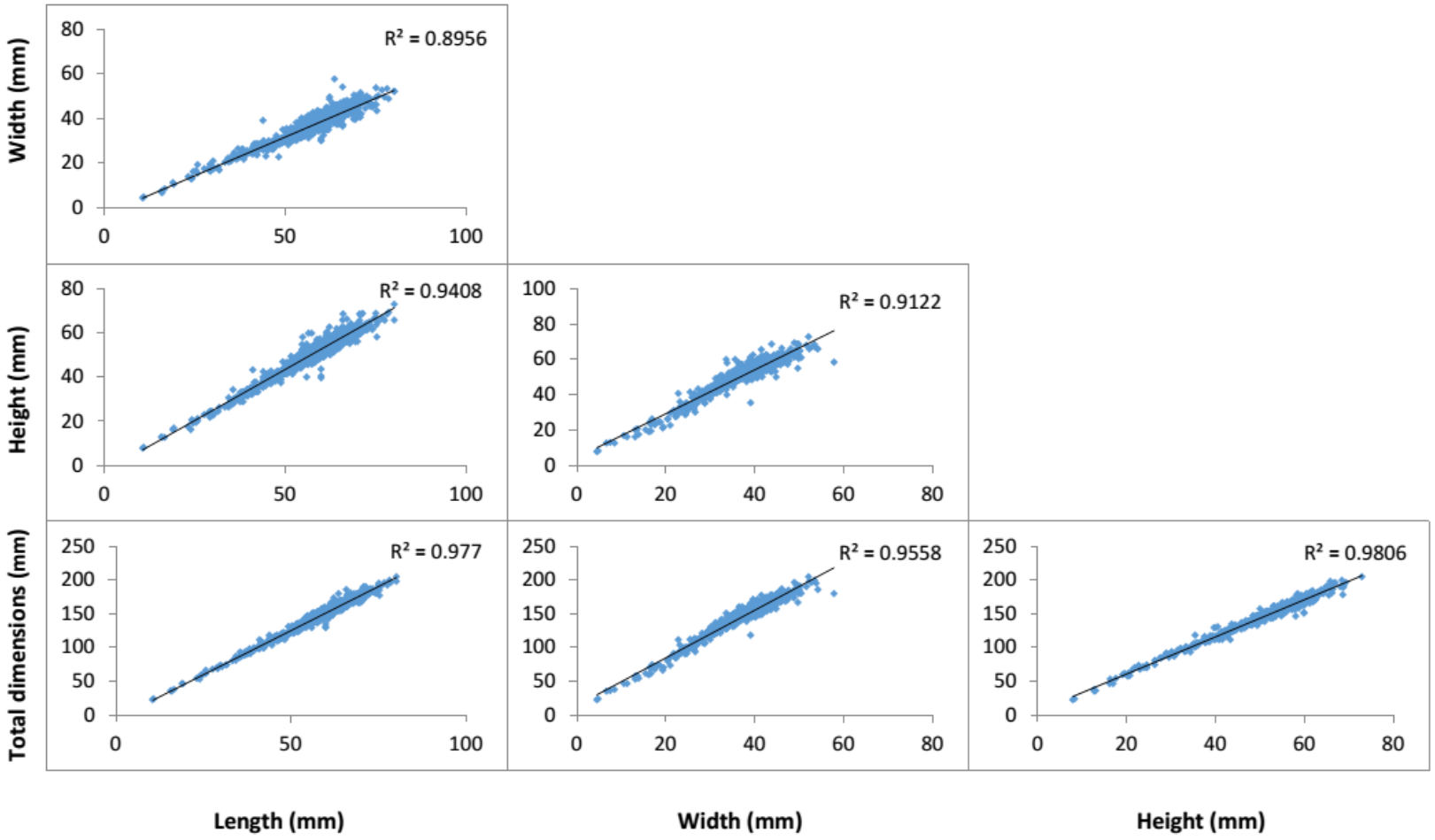

Figure 21. Scatterplot and fitted line of regression analysis between shell size parameters (Length, Width, Height and Total dimensions).

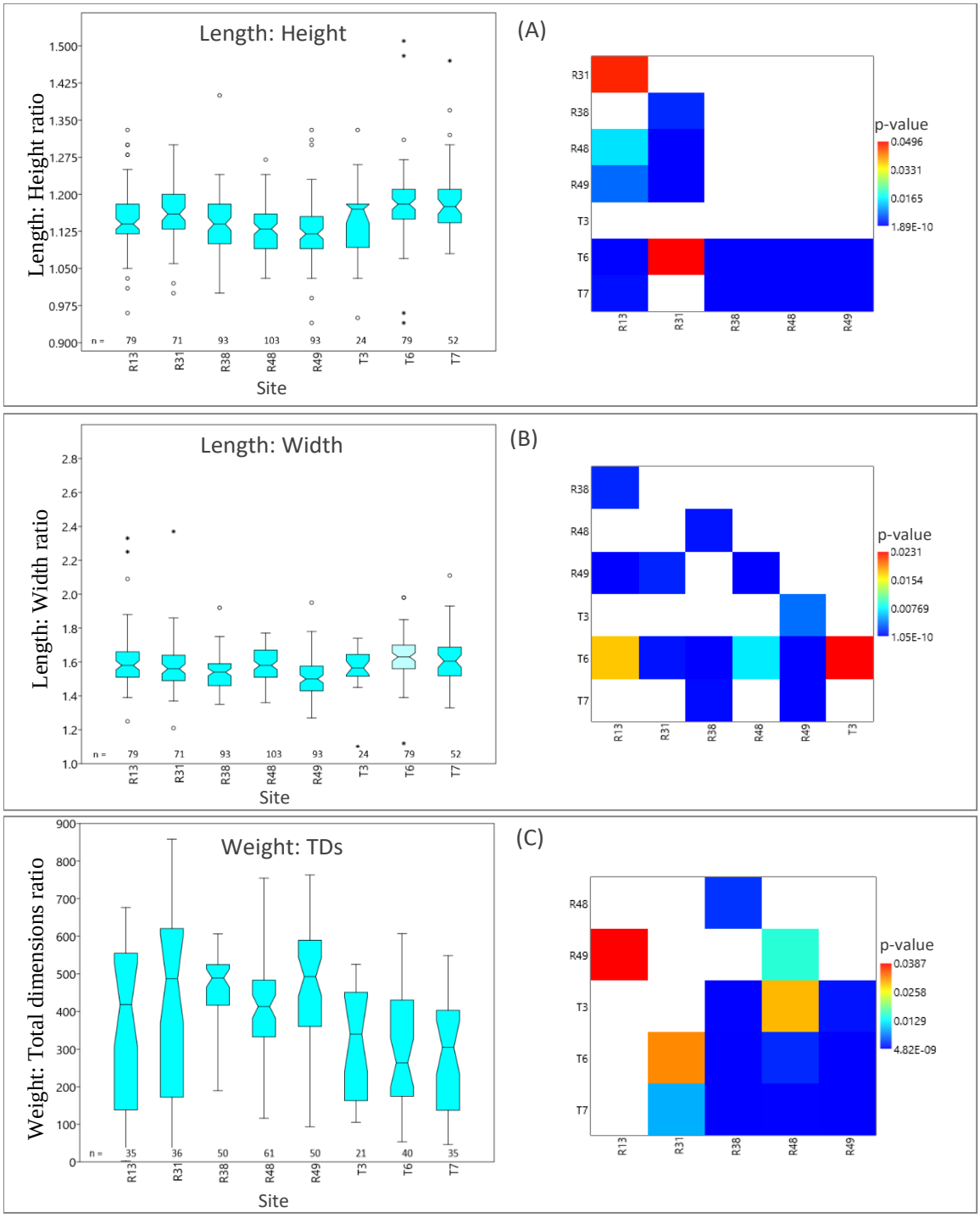

Figure 22. Variation in shell size variables by site calculated by Mann-Whitney pairwise test. A) Boxplot of Length: Height relationship by site. A) Boxplot of Length: width relationship by site. C) Boxplot of shell index (Weight: total dimensions, TD, relationship) by site. Matrix plots on (A), (B) and (C) show p-values for only sites with significantly different median (p-value < 0.05).

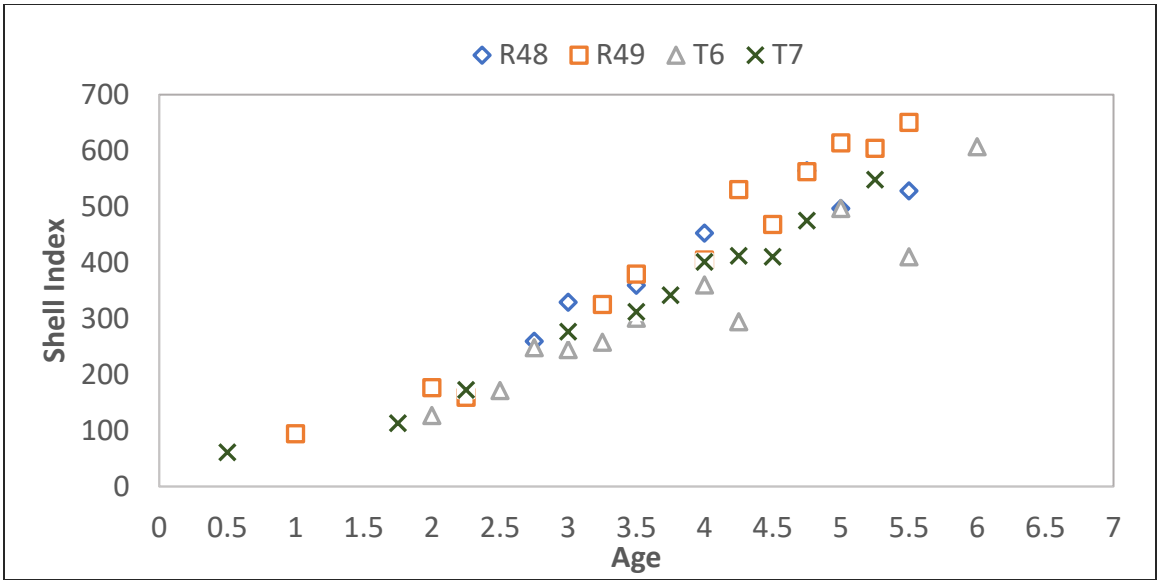

Figure 23. Shell index per age for selected sites (R49, R48, T6 and T7).

Shell microscopic structure

A total of 188 *R. cuneata* collected from July 2018, April 2019 and July 2019 were retained for sectioning. From these, a total of 133 *R. cuneata* were successfully sectioned, sanded, polished, microscopically examined and photographed. The remaining (55 of 188 *R. cuneata*) were either broken during preparation or the winter marks were indistinguishable.

For each year of growth, the increase in height was compared to the width of growth bands for each of 1st, 2nd and 3rd years of growth Significant correlation ($r = 0.39$, 0.40 and 0.56 respectively; $p < 0.001$) between annual increase in height and corresponding growth bands width was observed (Figure 24).

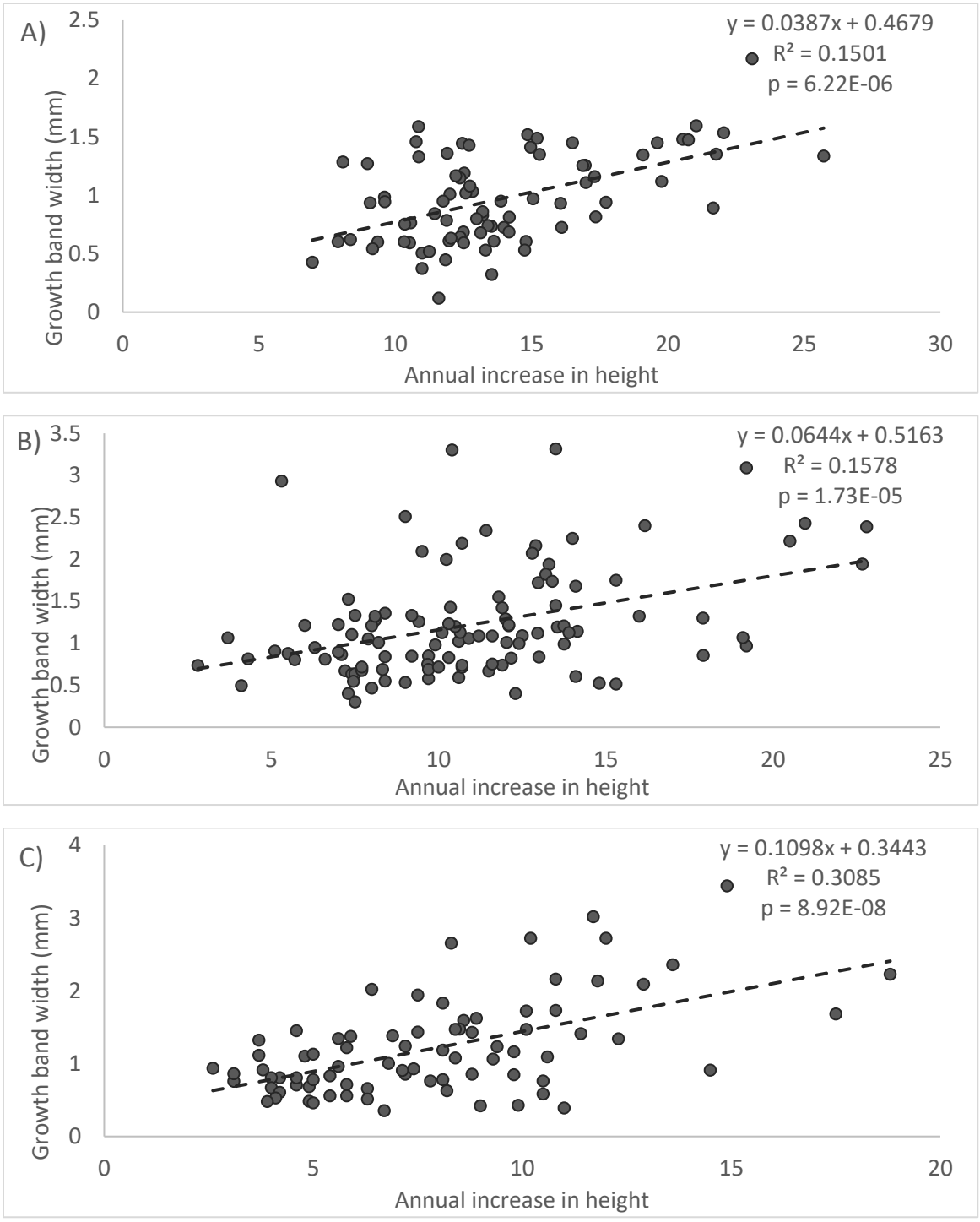

Figure 24. Regression between the annual increase in height (from spring to winter) and width of growth band formed concurrently during the same year for A) 1st complete year. B) 2nd complete year. C) 3rd complete year.

Influence of freshwater inflow on shell growth

In order to estimate the influence of freshwater discharge on the shell growth, the average increase in height during the complete year of growth (from spring to winter) was compared to the average freshwater inflow for the corresponding year. The year for averaging inflow was from April through March to cover the period when the annual growth takes place. During the 2015/2016 year, with the highest average freshwater inflow, the average increase in height for all years of growth was larger than increase in height took place in other years with lower average freshwater inflow. In contrast, the year 2017/2018, with relatively low average freshwater inflow exhibited lower average increase in height for all years of growth. (Figure 25). However, the average of each year of growth may be affected by what sites the *R. cuneata* were collected from. In other words, site effect needed to be investigated.

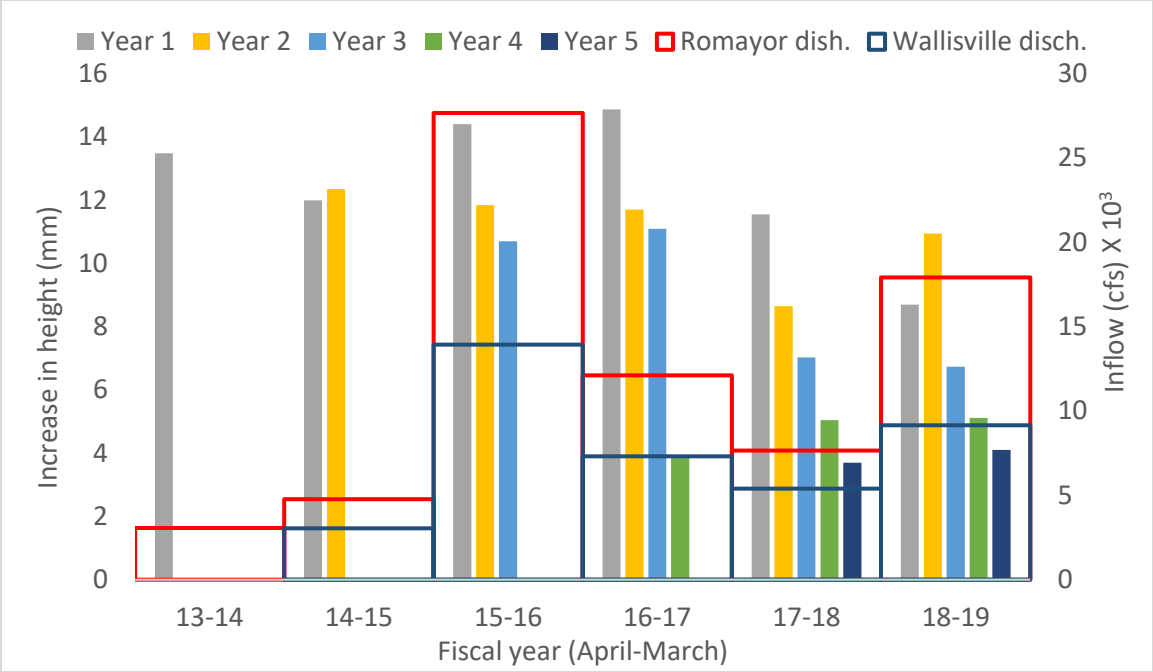

Figure 25. Annual increase in height (in different year of growths per different years) in relation to average inflow from Romayor and Wallisville gages. Romayor disch. = Discharge at Romayor. Wallisville disch. = Discharge at Wallisville.

Sites showed different rate of annual growth represented by the increase in height. As an example, mean annual increase in height in individual *R. cuneata* which completed their 1st year of growth during calendar year 2015-2016 were was different among sites (Figure 26). Results show clams from site R38 exhibited significantly lower growth than sites R48, T6 and R31. Site R49 seemed to have the largest median annual increase in shell height.

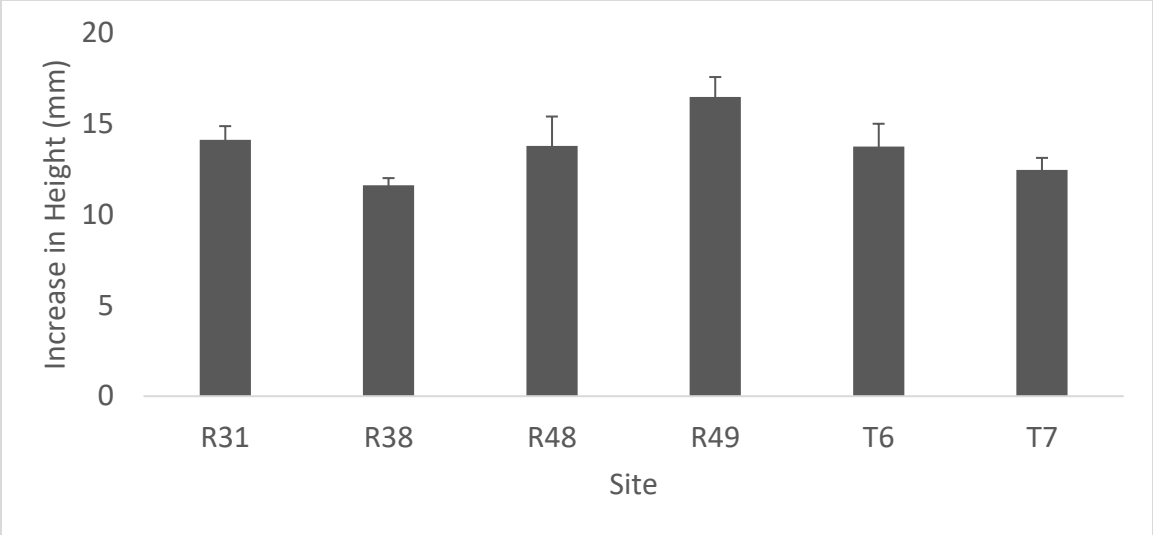

Figure 26. Mean increase in height during the first completed year of growth (year class) during 2015-2016 year.

Recruitment year and aging

The early growth (height at the first winter mark) data were collected for the 133 *R. cuneata* individuals. Due to limited number of sectioned *R. cuneata* individuals to be categorized according to site and recruitment year, data of height at first winter (of all *R. cuneata* individuals regardless site or recruitment year) were tested for bimodal distribution and the cutoff was calculated to be 18 mm Figure 27). This cutoff was used in aging where the early growth (heights at 1st winter mark) less than the cutoff (18 mm) was considered as "fall recruits" and added half a year to the completed years while early growth more than 18 mm were considered "spring recruits" and added one full year to the completed years.

Recruitment year determeination

Using reverse chronological rearrangement of winter marks data, recruitment years for examined *R. cuneata* were determined, i.e. a *R. cuneata* individual collected in summer 2018 with three complete year of growths was most likely recruited between spring 2014 through winter 2015 (Figure 28). Based on results from the aged sample of *R. cuneata*, years 2014-2015 and 2016-2017 (each from spring to next winter) had the highest number of recruited *R. cuneata* individuals.

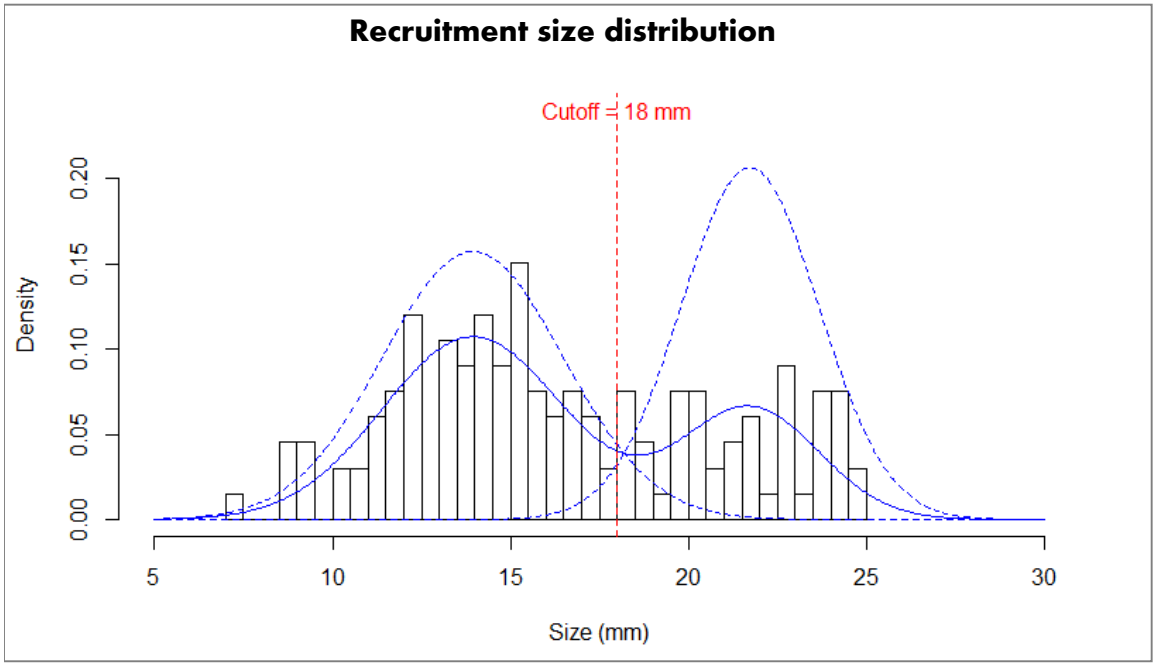

Figure 27. Bimodal distribution of height at 1st winter mark of aged *R. cuneata*. Solid blue line = Kernel density estimation of the distribution. Dashed blue line = probability distributions estimated by the expectation–maximization (EM) algorithm in the finite mixture model. Red dashed line = cutoff between spring and fall recruits.

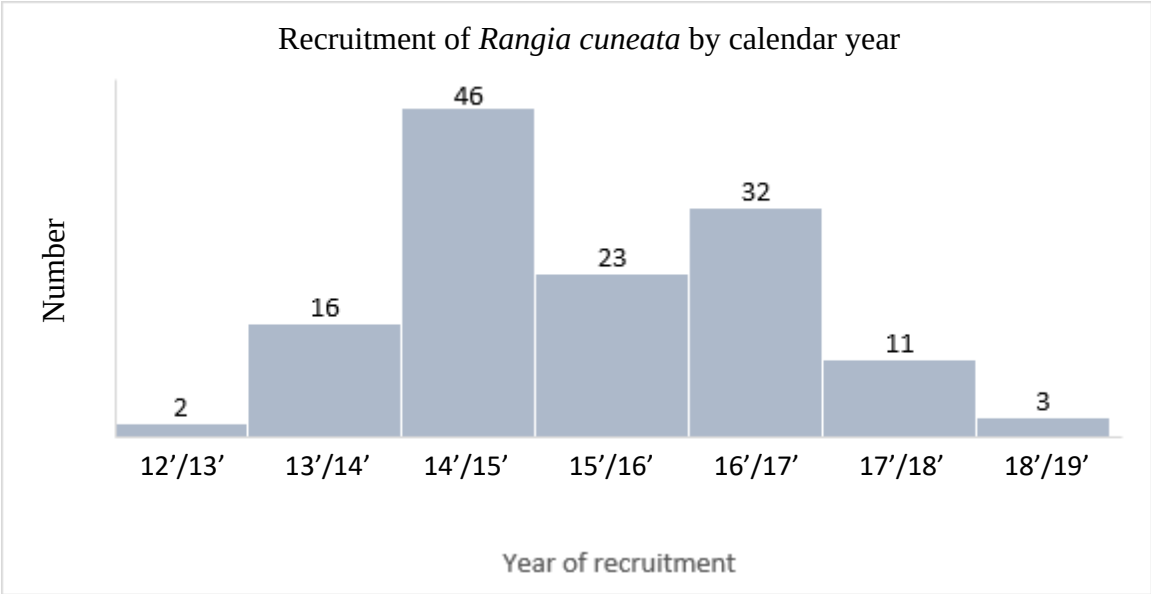

Figure 28. Distribution of aged *R. cuneata* by year of recruitment.

Fitting in von Bertalanffy growth model

Age data (from 133 *R. cuneata* individuals) were fitted in von Bertalanffy growth model with either length or total dimensions (TD) as shell size function (Figure *29*). Both age and dimensions data were fitted in the model with 95% confidence using PAST v 3.26 software.

Equation from von Bertalanffy growth model is valid for the whole *R. cuneata* population from the TRD and can be used to estimate length of individuals at a specific age using the following equation:

$$L = 99.325 * (1 - 0.88471 * e^{(-0.22047*(t))})$$

Where, $L_\infty = 99.325$, b = 0.88471, and k = 0.22047.

By rearranging this equation, the age (t) can be calculated from length (L) of any given individual *R. cuneata* from TRD population such that:

$$t = \frac{\ln(99.325) + \ln(0.88471) - \ln(99.325 - L)}{-0.22047}$$

This equation was applied to the individuals collected throughout the study that were not aged. The most abundant age of *R. cuneata* collected in this study in the TRD was 4 years (Figure 30).

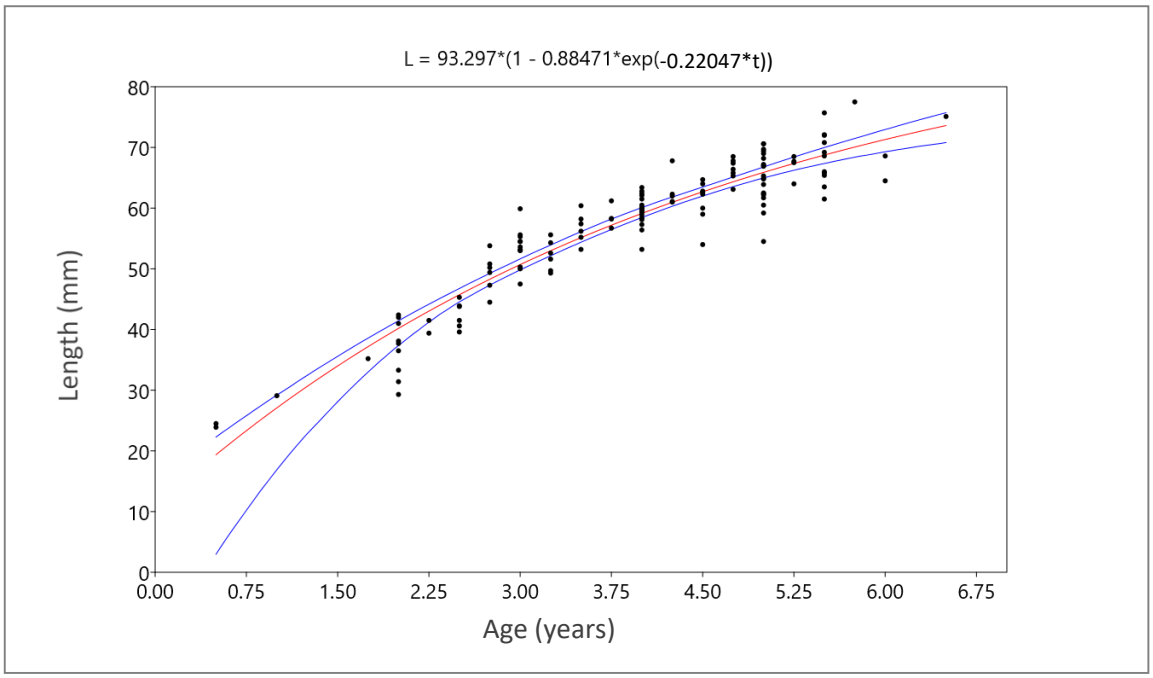

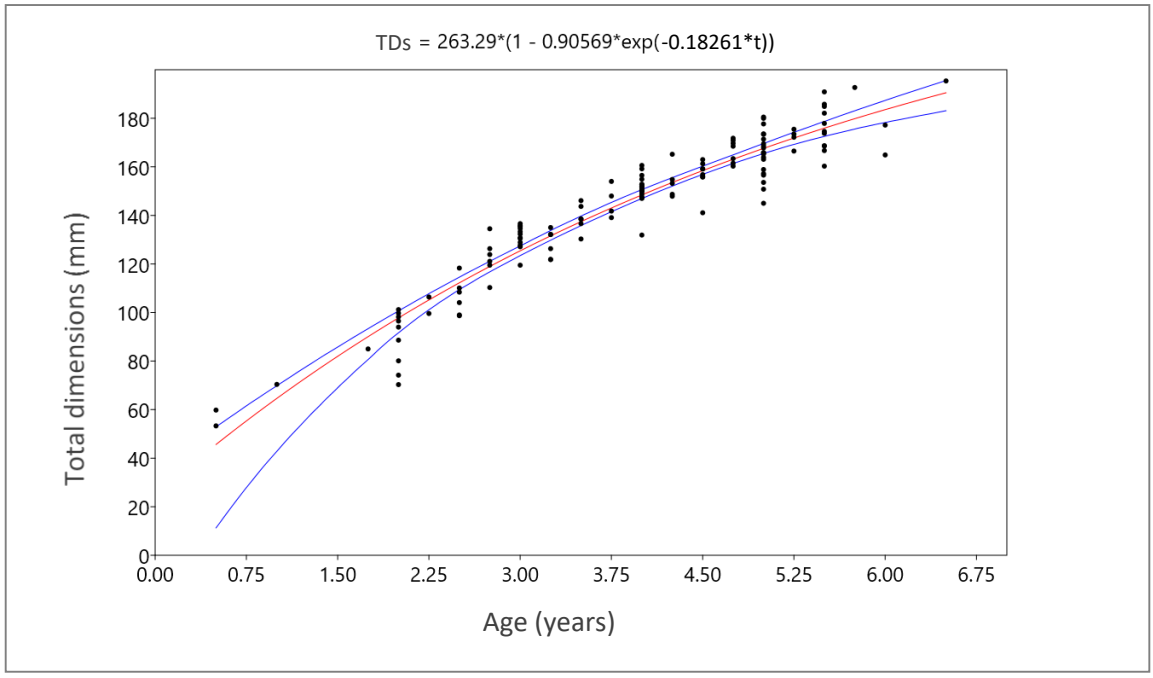

Figure 29. Age data fitted in von Bertalanffy growth model. A) Age versus length. B) Age versus total dimensions, TD.

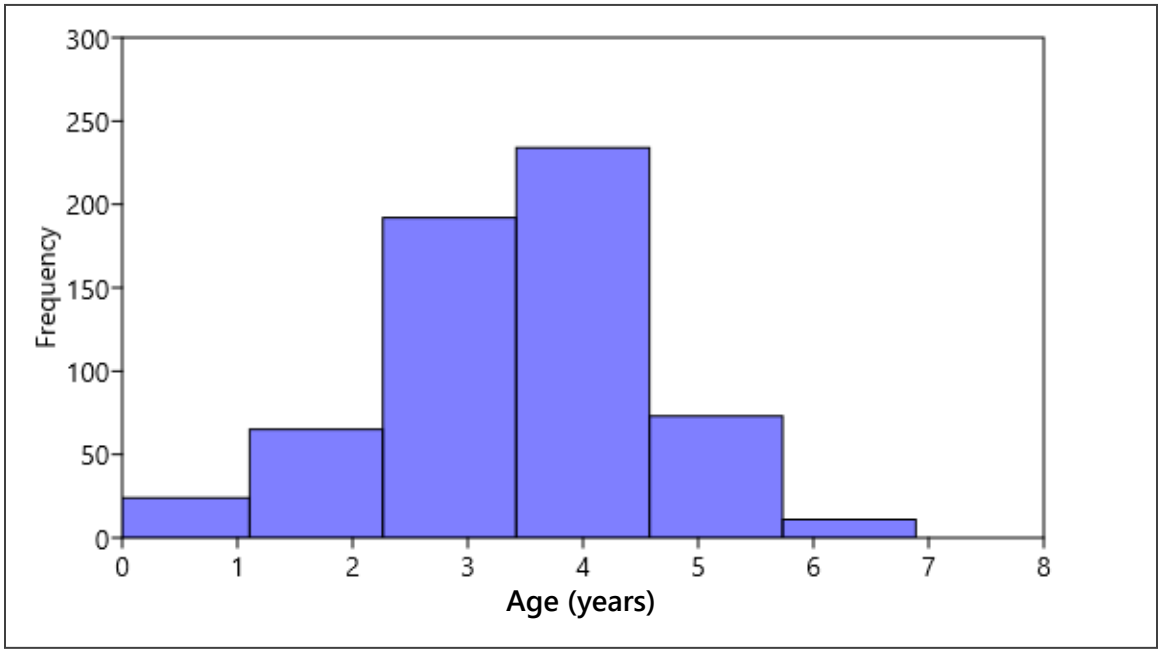

Figure 30. Distribution of estimated age for all *R. cuneata* collected throughout the study.

DISCUSSION

Environmental condition in the study area

Streamflow records of the Trinity River vary greatly from the upstream USGS gage at Romayor to the most downstream gage at Wallisville. In a study conducted by the USGS from May 2014 to December 2015, Lucena and Lee (2017) reported that streamflow at Wallisville made up only 54% of the total streamflow measured at upstream gages. This difference in streamflow was indicated to likely flow into wetland and water bodies connected to the main stream of Trinity River before Wallisville that makes about half of Trinity River streamflow gaged at upstream inflow into Galveston Bay indirectly through pathways other than Trinity River channel passing by Wallisville gage (Lucena and Lee, 2017). These diverted freshwater reaches TRD through the Old River.

The Old River discharge was monitored instantaneously by USGS during 9 high inflow events in the period between 2016 and 2019 to demonstrate that the measurements at the Old River site essentially accounted for the difference in discharge between Romayor and Wallisville gages (according to personal communications with Zulimar Lucena, Hydrologist at USGS and provided USGS unpublished data).

This was also was noted by comparing the stream inflow gaged at Romayor and Wallisville through this study period. The highest peak of streamflow recorded at Romayor was 78,100 cfs (on 10/20/2018) in contrast to the streamflow measured at Wallisville that never seemed to exceed 25,000 cfs (on 10/25/2018) regardless the upstream flow amount. This difference in discharge gaged at both gages may influence the salinity patterns in less predictable patterns then just straight-line distance to the mainstem river. This points out the importance of more understanding of the hydrology of Trinity River especially downstream within the delta. The threshold of inflow at which

this diversion takes place is important to understand for freshwater management. Also, the ecological importance of these wetlands and the Old River should be assessed in future studies which will give resource managers a more accurate evaluation of the impact of the freshwater outflow from Lake Livingston into the TRD.

Impact of freshwater inflow on sites local salinity and sediment type

The diversion of the flow during high flow events from the Trinity River makes it difficult to predict the correlation between local salinity at study sites and the freshwater inflow received from Trinity River at the Wallisville site. Local salinity at sites for the preceding 30, 60 and 90 days prior to sampling events were more affected by discharge gaged at Wallisville (significant strong negative correlation between average DSM and average freshwater inflow for the preceding 60 and 90 days) than discharge gaged at Romayor. This difference in effect of freshwater gaged at Romayor and Wallisville on local sites salinity is most likely explained by the lag time between the two gages (time required for the freshwater pulses to travel from Romayor to Wallisville). This lag time was measured during one of the elevated freshwater events during our study (during March 2018) to be more than 4 days. Also, this lag time seemed to inversely correlate with the size of the peak of freshwater pulse (Oakley et al, 2020). However, data-based modelling that takes in consideration other environmental variables (tides, wind, local precipitation, variation in depth) may better simulate the role that freshwater inflow plays in regulating salinity throughout the delta.

Sediment type, characterized by sediment percent fines, exhibited spatiotemporal variation. On the temporal level, variation in average percent fines of sediment samples collected from all sites on each sampling event was explained by variation in historical freshwater inflow gaged for the last 60 and 90 days at Romayor and Wallisville gage sites

prior to the sampling event. Also, on the spatial level, all sites exhibited negative correlation between measured sediment percent fines and the average freshwater inflow for the preceding 90 days. This negative relationship between sediment percent fines and the preceding freshwater inflow is most likely explained by the higher capacity of high flows to transport sand-size (not fine sediment) particles than low flows (Lucena and Lee, 2017).

As expected, many of the environmental parameters examined (salinity, percent fines, dissolved oxygen and water clarity) were found to be correlated with freshwater inflow. Dissolved oxygen was found to be higher on sampling events during high freshwater inflow than those sampling events in low freshwater inflow duration. Higher dissolved oxygen associated with high freshwater inflow can be explained by the flushing effect of high inflow that limits physical and biological factors which may reduce dissolved oxygen (Russell, 2006). In contrast to dissolved oxygen, water clarity measurements in durations of higher inflow were lower than those in low inflow durations. This can be explained by the increased water turbidity due to higher suspended sediment during high freshwater inflow durations.

Rangia cuneata population dynamics

Rangia cuneata abundance

Abundance is an indicator of long-term successful spawning and recruitment followed by survival and growth through years. Therefore, relating abundance to the environmental variables that were monitored for 18 months (this study duration) can be misleading. Total abundance of *R. cuneata* throughout this study varied among sites. Sites with the lowest average salinity had the fewest lowest abundance of *R. cuneata* while sites where *R. cuneata* abundance was the highest had the highest DSM.

Spatial variation in abundance explained by the degree of exposure to salinity fluctuation is supported by what we understand about how *R. cuneata* spawn. *Rangia cuneata* spawning is triggered by either sudden increase or drop in salinity (Cain, 1975; LaSalle and de la Cruz, 1985). Also, *R. cuneata* prefers a narrow salinity range for embryo (6-10 ppt) and larvae (2-20 ppt) survival (Cain 1973; Drescher, 2017). This range of salinity is less likely to happen in sites with less fluctuation in salinity. On a broader temporal scale, abundance of *R. cuneata* throughout Galveston Bay has been shown to increase during periods of higher salinity (Quigg and Steichen, 2015). Comparison of sites with different inflow regime can also be used to interpret abundance patterns.

Site R48 is on the mainstream of the channelized part of Trinity River where continuous flow is secured even in lower inflow periods. This continuation in inflow may be the reason for surviving of all *R. cuneata* at this site. While site R49 is not located on the mainstream of Trinity River, but rather on Old River, which receives inflows from wetlands and water bodies that mentioned previously only receive the overflow from upstream parts of Trinity River during high inflow events. With this intermittent inflow regime, Old River seems to provide inferior habitat for *R. cuneata*. This potential explanation for the high percentage of dead *R. cuneata* at site R49 is supported by Johns (2012) where he documented the wide-spread mortality of *R. cuneata* in the upper portion of the Guadalupe Estuary after the drought of 2011.

Meat Index as health indicator

A high value of MI indicates more favorable environmental conditions while a low value suggests poor conditions (Tenore et al., 1968). Butler (1952) stated that MI is best used as a health assessment when comparing individuals within a population collected during a particular time (Tenore et al. 1968). MI shows quick and short-term response to change in environmental conditions, which can affect *R. cuneata* health (Nishida et al., 2006).

Variations of MI for a population can vary if any subpopulations are exposed to different degrees of environmental stressors. In this study, some sites were significantly higher in average MI than other sites. Meat index can be a useful allometric relationship in studying environmental effects on bivalves. Average MI of a population can be affected by the average size of its individuals. This effect is explained by the more likelihood of juvenile *R. cuneata* to accumulate more meat than adult *R. cuneata*. Therefore, a population with high percentage of Juveniles will have larger average MI than a population with low juvenile percentage.

Influence of environmental conditions on meat index

Among the environmental variables tested for their relationship with MI, only sediment percent fines and average DSM for the last 60 and 90 days were significantly negatively correlated to average MI for each site. Negative correlation between MI and average DSM explains the stressful effect of fluctuating salinity on MI, i.e. the wider the daily range of salinity the clam is exposed to, the less MI accumulated. Although MI didn't show significant statistical correlation with historical inflow (for 30, 60 and 90 days), the fact that negative correlation between MI and freshwater inflow proxies

(salinity and sediment, negatively correlate with freshwater inflow) implies the positive relationship between inflow and MI.

The negative relationships between salinity as a proxy of freshwater inflow and MI are well reported in literature (Parnell et al, 2011; Guillen et al., 2016). Moreover, for the TRB *R. cuneata* population, this negative relationship becomes obvious when comparing previous recent studies with the current study. In the last decade three surveys have been conducted on the distribution and health of *R. cuneata* in Trinity Bay. These studies were conducted within different inflow regimes which ranged from drought (low inflow) to wet conditions. According to records of average outflow from Livingston Dam (Upstream dam on Trinity River whose outflows control inflow along Trinity River downstream from the dam) for the period from 1965 through 2015, years 2011 then 2014 were the two lowest years in this period while 2015 was the highest year with outflows from the dam (Lucena and Lee, 2017).

Matching the different inflow regimes on these years, average MI reported in studies conducted in 2011, 2012 and 2014 were 12.5, 11.5 and 11.2, respectively (Parnell et al., 2011; Windham, 2015). Guillen et al (2016) recorded the highest compared to all studies with average MI 30.3 This study was conducted within a period when average inflow was higher than 2011-2014 average inflow but less than 2016 average inflow. Average MI was 22 for this study. There appears to be a clear trend between the health of the *R. cuneata* population in the TRD and the recent freshwater inflow patterns of the Trinity River.

Rangia cuneata had higher MI when found in sediment with low percent fines (sandy sediment) than when grown in sediment with high percent fines (Clay-silt sediment) (Tenore et al., 1968). As mentioned previously, percent fines of sediment had

an inverse relationship with freshwater inflow, therefore periods of high inflow result in decreased percent fines, which results in an increased MI of *R. cuneata*.

Along with sediment, freshwater inflow events are important for delivering nutrients (nitrogen and phosphorus) to the TRD. During a study conducted in 2014-2015, Lucena and Lee (2017) found that the average nutrients concentration in high inflow events was 75% higher than average nutrients concentrations in low inflow events. The source of these nutrients was interpreted to be caused by a combination of transported nutrient from Lake Livingston and the upper Trinity River watershed, and mobilization of sediment-attached nutrients stored in the lower Trinity River channel and watershed under the effect of high inflow.

Shell structure and aging

Shell dimensions and weight

Three conventional shell dimensions were used to measure *R. cuneata* size, length, height and width. Interestingly, the ratio between shell length and other shell dimensions (i.e. length: width and length to height) varied among and within sites. For example, most *R. cuneata* collected form site T6 had significantly larger length: width and length: height ratios than *R. cuneata* collected from other sites. This irregularity in ratios between dimensions can be overcome by using the TD instead of any single dimension. This suggestion is based on the fact that the regression between the total shell dimensions, TD, and each of other shell dimensions (length, width and height) yields higher coefficient of determination, R^2, than regression between any of these three dimensions and each other. The TD can be used to help decrease the natural variation among *R. cuneata* individuals and represent the shell size more accurately. Based on

these results, I recommend the use of the total dimensions, TD, as a more accurate representation of the shell size.

Furthermore, we first introduce the "shell index" as a valid long-term growth variable. Shell index is the ratio of shell weight to shell TD. This consideration was based on the observation that some shells are thicker and heavier than others for the same size range. It is based on the assumption that the thickness and weight of a shell is a function of how well-fed and less stressed this *R. cuneata* individual is. Unlike MI, shell index can be used as long-term health indicator.

Sites R38, R48, and R49 had significantly higher shell index than sites T3, T6 and T7. This clustering of sites is quite similar to the way these sites are clustered based on abundance. It seems that the combination of environmental conditions at sites R38, R48 and R49 not only supports abundance but also enhances *R. cuneata* health represented by higher shell index.

The relationships between *R. cuneata* shell weight and both age and length were studied by Black and Heaney (2015) in their investigation of *R. cuneata* in three Texas Bays: Mission Lake, Trinity Bay and Sabine Lake. *Rangia cuneata* collected from Mission Lake seemed to have higher shell weight for the same age and length than Trinity Bay and Sabine Lake. Variation in this relationship among bay systems and within the bay (current study) qualifies it to be a good variable to monitor long term growth pattern in TRD and other estuarine systems.

Shell microscopic structure

The shell growth took place during a given year of growth was measured by the increase in height and the width of growth band formed during this year. Comparisons between annual increase in height and the width of corresponding inner layer growth

bands showed limited correlation. Since the growth rate in both layers were not perfectly correlated, and based on what was mentioned by Surge and Schöne (2015) about the reversibility of inner layer, annual growth rate of was measured by the annual increase in height (height at a winter mark minus height at the preceding winter mark).This increase in height is a function of annual growth under different conditions.

To investigate the effect of annual variation in freshwater inflow on the annual increase in height, the average increase in height happened throughout different years of growth (1^{st}, 2^{nd}, 3^{rd}, …. etc. year of age) were compared to the average inflow throughout the calendar year during which the year of growth was spent. Calendar years with high freshwater inflow (e.g. the year 2015-2016) supported higher annual increase in height for all years of growth compared to calendar years with lower freshwater inflow (e.g. 2017-2018) that supported lower annual increase in height for the same years of growth.

Although these differences were not tested for significance, these results describe a positive relationship between the shell growth rate, represented by increase in height, and average inflow received during the year when this growth was taking place. The use of a 2-way nested or mixed model for evaluating growth versus cohort, age, location, and environmental variables should be considered during future studies designed to detect the influence of freshwater inflow on *R. cuneata* growth (Weisberg et al 2010).

Shells from different sites were shown to grow at different annual rates. Some sites had significantly higher annual increase in height than other sites for the same year of growth during the same calendar year. For example, the average increase in height for *R. cuneata* individuals which lived their 1^{st} year of growth during 2015-2016 varied among sites. Sites R49 and R48 seemed to have higher increase in height than other sites. Again, sites with higher annual increase in height are generally the same sites with higher abundance and higher shell index.

Variation among sites in these growth variables (annual increase in height, shell index and abundance) is most likely explained by their location within the delta, i.e. proximity or distance from the main river stream and from the open bay; both which determine the magnitude of salinity the site is exposed to. Sites with high daily magnitude of salinity are 1) more exposed to different degrees of water chemistry and concentrations of minerals that can play a critical role in shell deposition and consequently growth, and 2) more susceptible to salinity spikes even with slight drops in freshwater inflow. This can increase the likelihood and improve the timing of spawning.

Determination of recruitment year and age

Age detemination

Age determination has many challenges to overcome including the subjectivity of where to precisely assign winter marks. Another challenge is to estimate the age of the early and late growth before and after the completed years. The late growth after the last winter mark is easier to determine, as it is dependent on when the individual was collected, but the early growth remains more difficult to estimate.

Typically, this early growth is variable depending on the timing of larval production and settlement, and subject to differences in growing conditions at the place of settlement (Jacobson et al., 2006). *Rangia cuneata* is well known for spawning twice a year in almost all studies conducted in estuaries on the GOM (Cain, 1975; LaSalle et al., 1985).

As such, I suggest that it is acceptable to estimate the season of recruitment (spring or fall) depending on the bimodal distribution of the height at the first winter data. In future studies, I recommend testing for bimodal distribution based on the recruitment year by site. The most accurate way to estimate the age of the early growth is to test each

sites' recruits for the same year of recruitment for bimodal distribution. The primary limitation to this approach is that it requires a larger sample size.

Recruitment year

Recruitment year of a given clam was calculated by reverse chronological arrangement of winter marks data, i.e. a clam collected in summer 2018 with three complete year of growths was most determined to be recruited between spring 2014 and winter 2015. Distribution of *R. cuneata* recruitment among years shows that the 2014-2015 and 2016-2017 years had the highest number of recruited *R. cuneata*. In contrast the 2015-2016 year had a lower ratio of recruitment. This difference in recruitment among years is most likely explained by the variation freshwater inflow. Assuming these numbers of recruited *R. cuneata* per year are representative to the overall recruitment that occurred throughout the TRD in these years, the year 2014-2015 supported the most successful recruitment year. Interestingly, the 2014-2015 year is one of the two lowest inflow years on record (Lucena and Lee, 2017).

Rangia cuneata spawning and recruitment has been shown to be sensitive to salinity level (Cain 1975; LaSalle et al, 1985, Drescher, 2017, Johns 2012). These critical salinity levels are more likely to happen in dry years than in wet years. Periods of high freshwater inflow lowered salinity at most of sites to almost 0 ‰ during this study. During these periods of low salinity, spawning is less likely to be triggered and low survival of embryos and larvae is predicted. In conclusion, dry years may affect the *R, cuneata* health on the short-term, but they are important for successful spawning and recruitment, especially in parts of the TRD where freshwater inflow is continuous like the main Trinity River channel.

Distribution of age

Data of determined age and length were fitted in Von Bertalanffy Growth model. The output function was derived according to Fabens' equation. This equation is mathematically arranged to measure length (L) when the age (t) is known. I rearranged the output formula to measure the age from measured length. The rearranged formula was applied to all the collected *R. cuneata* throughout the study to determine the age using the length data.

Age data have shown that the majority of *R. cuneata* fall in age 3-4 years old. This can be an indicator that the population is still growing and follow a normal distribution with all age cohorts represented. This distribution of age cohorts indicates successful long-term recovery from the drought period between 2011 and 2014.

The oldest aged individuals were 6.5-7 years old throughout the study. With different results, in their study of three estuarine systems among which Trinity Bay was studied, Black and Heaney (2015) reported *R. cuneata* live individuals with 10 years and dead-collected individuals with up to 12 years old. Interestingly, shell length in Black and Heaney (2015) did not exceed 60 mm and 70 mm for live and dead-collected *R. cuneata* respectively. Maximum shell length throughout this study was 78.6 mm and 80.1 mm for live and dead-collected *R. cuneata*, respectively.

However, by applying Black and Heaney's aging method and this study's method on a given clam, this study's method should yield a larger age since it considers the age of early and late growth while Black and Heaney's method does not. This difference between the population aged by Black and Heaney and this study's population, in terms of age/size relationship, may be explained by either the long-term freshwater inflow regime each population experienced or the location from where the *R. cuneata* individuals were collected during each study.

Conclusion and future recommendation

Rangia cuneata is a responsive indicator species to multiple metrics that are directly related to freshwater inflows within the TRD. This study was the first to utilize continuous monitoring of environmental conditions. i.e. salinity and temperature while monitoring seasonal *R. cuneata* populations. Availability of these time series of environmental data is a good start to understand how the environmental variables in the TRD correlate to each other and how they impact the health of *R. cuneata*. While MI is a short-term metric to measure clam health, shell growth can be used to measure long-term clam health. Shell index (the ratio of shell weight to total dimensions of shell) is recommended as a valid long-term health indicator.

Future recommendations include further continuous monitoring of environmental conditions throughout the delta and quarterly sampling of *R. cuneata* to help better understand the response of *R. cuneata* to freshwater inflow. The use of mark-recapture methods in on-site cages for *R. cuneata* can help elucidate growth rates of individuals at sites through time. Moreover, hydrodynamic modeling of inflow throughout the delta will be a powerful tool to understand this complicated environment more clearly.

REFERENCES

Black, B.A. and M. Heaney, 2015. *Rangia* Clam Investigations. Texas Water Development Board, Austin, TX, p. 46.

Cain, T., 1973. The combined effects of temperature and salinity on embryos and larvae of the clam *Rangia cuneata*. Marine Biology 21, 1-6.

Cain, T., 1975. Reproduction and recruitment of the brackish water clam *Rangia cuneata* in the James River, Virginia. Fishery Bulletin 73, 412-430.

Chambers, J.M., 1983. Graphical methods for data analysis. Wadsworth International Group, Belmont, Calif.

Drescher, B., 2017. An Ecological Examination of Johnson Bayou (Pass Christian, MS) With a Reproductive Histological Analysis of *Rangia cuneata*, and a Comparative Morphological Study of the Foot and Shell of *Rangia cuneata* and *Polymesoda caroliniana*.

Fabens, A.J., 1965. Properties and fitting of the Von Bertalanffy growth curve. Growth 29, 265-289.

Fritz, L., L. Ragone, and L. Lutz, 1990. Microstructure of the outer shell layer of *Rangia cuneata* (Sowerby, 1831) from the Delaware River: Applications in the studies of population dynamics. J. Shellfish Res 9, 205-213.

Ginn, T., S. Becker, and J. Green. 1990. Technical Memorandum to EPA from PTI: Reconnaissance Survey of Reference Area Sediments in Shallow Waters of Carr Inlet. PTI, Seattle, WA.

GISD, 2020. Global Invasive Species Database (2020) Species profile: *Rangia cuneata*.

Guillen, G., A. Gordon, J. Oakley, and M. Mokrech, 2016. Trinity River Delta and Upper Trinity Bay Rangia Population Assessment. University of Houston-Clear Lake, Houston, TX, p. 58.

Jacobson, L.D., S.J. Sutherland, J. Burnett, M.M.C. Davidson, J.M. Harding, J. Normant, A. Picariello, and E.N. Powell. 2006. Report from the Atlantic surfclam (Spisula solidissima) Aging Workshop Northeast Fisheries Science Center, Woods Hole, MA, 7-9 November 2005.

Johns, N.D., 2012. Examining bay salinity patterns and limits to *Rangia cuneata* populations in Texas estuaries. National Wildlife Federation.

Ko, J.Y. and S.R., Johnston, 2007. The Economic Value of Ecosystem Services Provided by the Galveston Bay/Estuary System.

LaSalle, M.W. and A.A., de la Cruz, 1985. Species Profiles: Life Histories and Environmental Requirements of Coastal Fishes and Invertebrates (Gulf of Mexico): COMMON RANGIA. U.S. Fish and Wildlife Service and U.S. Army Corps of Engineers, Biological Report 82 (11.31), 18p.

Lever, J., M. Krzywinski and N. Altman, 2017. Principal component analysis. Nature Methods 14, 641-642.

Lucena, Z. and M.T. Lee, 2017. Characterization of streamflow, suspended sediment, and nutrients entering Galveston Bay from the Trinity River, Texas, May 2014–December 2015, Scientific Investigations Report, Reston, VA, p. 49.

MacFarland, T.W. and J.M. Yates, 2016. Mann–whitney u test, Introduction to nonparametric statistics for the biological sciences using R. Springer, pp. 103-132.

McKight, P.E. and J. Najab, 2010. Kruskal-wallis test. The corsini encyclopedia of psychology, 1-1.

Nielsen-Gammon, J.W., 2012. The 2011 texas drought. Texas Water Journal 3, 59-95.

Nishida, A.K., N. Nordi, and R.R. Alves, 2006. Molluscs production associated to lunar-tide cycle: A case study in Paraíba State under ethnoecology viewpoint. Journal of Ethnobiology and Ethnomedicine 2, 28.

Oakley, J.W., M.E. Omar, and G.J. Guillen. 2020 (In Review). Characterization of the Influence of Freshwater Inflow on Trinity River Delta Bioindicators. EIH Report 20-001 submitted to the Galveston Bay Estuary Program in partial fulfillment of contract: 582-18-80338. pp 57.

Parnell, A., R. Windham, S. Ray, A. Schulze, and A. Quigg, 2011. Distribution of Rangia clams in response to freshwater inflows in Galveston Bay, Texas, Final Report to Texas Parks and Wildlife Award, p. 49.

Pulich Jr, W., 2007. Galveston Bay System. Seagrass Status and Trends in the Northern Gulf of Mexico: 1940–2002, 17-28.

Quigg, A. and J. Steichen, 2015. Defining Bioindicators for Freshwater inflow Needs Studies. Texas A&M University at Galveston, p. 139.

Razali, N.M., and Y.B.Wah, 2011. Power comparisons of shapiro-wilk, kolmogorov-smirnov, lilliefors and anderson-darling tests. Journal of Statistical Modeling and Analytics 2, 21-33.

Russell, M.J., 2006. Effect of freshwater inflow on net ecosystem metabolism in Lavaca Bay, Texas. Estuarine, Coastal and Shelf Science.

Scheff, S.W., 2016. Chapter 8 - Nonparametric Statistics, in: Scheff, S.W. (Ed.), Fundamental Statistical Principles for the Neurobiologist. Academic Press, pp. 157-182.

Surge, D. and B.R. Schöne, 2015. Bivalve sclerochronology. Encyclopedia of Scientific Dating Methods. Springer, Dordrecht, 108-115.

Tenore, K.R., D.B. Horton, and T.W. Duke, 1968. Effects of bottom substrate on the brackish water bivalve *Rangia cuneata*. Chesapeake Science 9, 238-248.

TSJ-BBASC, 2012. Work plan report. Trinity and San Jacinto and Galveston Bay Basin and Bay Area Stakeholder Committee and Expert Science Team.

TSJ-BBEST, 2009. Trinity and San Jacinto and Galveston Bay Basin and Bay Expert Science Team, in: TCEQ (Ed.), Environmental Flows Recommendations Report, Austin, TX.

Wakida-Kusunoki, A.T. and C.L. MacKENZIE Jr, 2004. Rangia and Marsh clams, *Rangia cuneata*, *R. flexuosa*, and *Polymesoda caroliniana*, in eastern Mexico: distribution, biology and ecology, and historical fisheries. Marine Fisheries Review 66, 13-20.

Weisberg, S., G.R. Spangler and L. Richmond. 2010. Mixed effects models for fish growth. Canadian Journal of Fisheries and Aquatic Sciences 67(2):269-277.

Windham, R., 2015. Rangia as potential indicators of bay health. College Station, Texas: Texas A&M University, Master's thesis, 83p.

Wong, W.H., N.N. Rabalais, and R.E. Turner, 2010. Abundance and ecological significance of the clam *Rangia cuneata* (Sowerby, 1831) in the upper Barataria Estuary (Louisiana, USA). Hydrobiologia 651, 305-315.

APPENDIX:

RESULTS OF STATISTICAL ANALYSIS

Table 13. Correlation coefficient (r, black text color) and significance (p-value, red text color) output of meat index correlation with salinity and inflow variables calculated in PAST v 3.26. Median MI = median meat index. Salinity (DSM)/ (n) = Average daily salinity magnitude for n number of days. Roma. / Wallis. disch. (n) = average of historical discharge (inflow) from Romayor or Wallisville gage for n number of days.

	Median MI	Salinity (DSM) 90	Salinity (DSM) 60	Salinity (DSM) 60	Roma. disch. 90	Roma. disch. 60	Roma yor disch. 30	Wallis. disch. 90	Wallis . disch. 60	Wallis . disch. 30
Median MI		0.01	0.00	0.06	0.26	0.71	0.47	0.06	0.69	0.86
Salinity (DSM) 90	-0.48		0.00	0.01	0.00	0.13	0.64	0.00	0.01	0.26
Salinity (DSM) 60	-0.49	0.94		0.00	0.00	0.02	0.12	0.00	0.00	0.02
Salinity (DSM) 60	-0.32	0.49	0.72		0.00	0.00	0.00	0.00	0.00	0.00
Roma. disch. 90	0.19	-0.58	-0.64	-0.62		0.00	0.00	0.00	0.00	0.00
Roma. disch. 60	-0.06	-0.28	-0.39	-0.57	0.80		0.00	0.00	0.00	0.00
Roma. disch. 30	-0.12	-0.09	-0.26	-0.55	0.72	0.97		0.00	0.00	0.00
Wallis. disch. 90	0.31	-0.68	-0.73	-0.71	0.96	0.75	0.64		0.00	0.00
Wallis. disch. 60	0.07	-0.43	-0.53	-0.73	0.81	0.95	0.89	0.84		0.00
Wallis. disch. 30	-0.03	-0.21	-0.37	-0.72	0.71	0.93	0.94	0.71	0.96	

Table 14. Correlation coefficient and p-value for MI versus salinity variables, inflow variables (average flow for previous 60 and 90 days) and sediment percent fines. Avg. DSM/ (n) days = Average daily salinity magnitude over the previous number of days. Corr. coef. = correlation coefficient. Roma. = Romayor gage. Wallis. = Wallisville gage.

Site	Avg. DSM/ 90 days		Avg. DSM/ 60 days		Freshwater Inflow (Corr. coef., r)				Sediment (fine %)	
	Corr. coef., r	p-value	Corr. coef., r	p-value	Roma. 90 days	Roma. 60 days	Wallis. 90 days	Wallis. 60 days	Corr. coef., r	p-value
R13	-1.00	0.006	-0.97	0.026	0.94	0.56	0.91	0.57	-0.80	0.199
R31	-0.97	0.033	-0.91	0.030	0.72	0.46	0.76	0.47	-0.33	0.593
R38	-0.32	0.678	-0.34	0.571	0.21	-0.38	0.23	-0.31	-0.07	0.916
R48	-0.55	0.337	-0.41	0.424	0.24	-0.24	0.37	-0.09	-0.30	0.557
R49	-0.46	0.538	-0.47	0.422	-0.17	-0.06	0.01	0.10	-0.71	0.175
T3	-0.34	0.780	-0.29	0.810	-0.63	-0.83	-0.39	-0.67	-0.89	0.305
T6	-0.85	0.147	-0.52	0.479	0.26	-0.18	0.52	0.25	-0.27	0.733
T7	-0.76	0.132	-0.67	0.219	-0.10	-0.38	0.09	-0.19	-0.08	0.896

Table 15. Multiple regression models output for regression between MI and environmental variables. A) Meat index versus average salinity magnitude for the last 60 days. B) MI versus average salinity magnitude (60 days) and sediment percent fines. C) MI versus average salinity magnitude (60 days), sediment percent fines and temperature

A) MI versus Average salinity magnitude for the last 60 days

Regression Statistics	
Multiple R	0.486
R Square	0.236
Adjusted R Square	0.214
Standard Error	2.760
Observations	37

ANOVA

	df	*SS*	*MS*	*F*	*Significance F*
Regression	1	82.500	82.500	10.828	0.002
Residual	35	266.662	7.619		
Total	36	349.163			

	Coefficients	*Standard Error*	*t Stat*	*P-value*	*Lower 95%*	*Upper 95%*	*Lower 95.0%*	*Upper 95.0%*
Intercept	22.860	0.590	38.737	0.000	21.662	24.058	21.662	24.058
Avg. magnitude 60	-2.343	0.712	-3.291	0.002	-3.789	-0.898	-3.789	-0.898

B) MI versus average salinity magnitude (60 days) and sediment percent fines

Regression Statistics	
Multiple R	0.530
R Square	0.281
Adjusted R Square	0.238
Standard Error	2.718
Observations	37

ANOVA

	df	*SS*	*MS*	*F*	*Significance F*
Regression	2	98.019	49.010	6.635	0.004
Residual	34	251.144	7.387		
Total	36	349.163			

	Coefficients	*Standard Error*	*t Stat*	*P-value*	*Lower 95%*	*Upper 95%*	*Lower 95.0%*	*Upper 95.0%*
Intercept	25.268	1.208	20.921	0.000	22.813	27.722	22.813	27.722
Avg. magnitude 60	-0.875	0.424	-2.063	0.047	-1.738	-0.013	-1.738	-0.013
% fines	-0.060	0.023	-2.571	0.015	-0.107	-0.013	-0.107	-0.013

C) MI versus average salinity magnitude (60 days), sediment percent fines and temperature

Regression Statistics	
Multiple R	0.634
R Square	0.401
Adjusted R Square	0.347
Standard Error	2.517
Observations	37

ANOVA

	df	*SS*	*MS*	*F*	*Significance F*
Regression	3	140.180	46.727	7.379	0.001
Residual	33	208.982	6.333		
Total	36	349.163			

	Coefficients	*Standard Error*	*t Stat*	*P-value*	*Lower 95%*	*Upper 95%*	*Lower 95.0%*	*Upper 95.0%*
Intercept	23.697	1.586	14.938	0.000	20.469	26.924	20.469	26.924
Salinity (DSM) 60	-2.420	0.712	-3.397	0.002	-3.869	-0.970	-3.869	-0.970
% fines	-0.066	0.023	-2.935	0.006	-0.112	-0.020	-0.112	-0.020
Temp. 60	0.108	0.071	1.529	0.136	-0.036	0.252	-0.036	0.252

Table 16. Regression model for increase in height and growth band width as growth variables during the 1st complete year of growth.

Regression Statistics	
Multiple R	0.387487
R Square	0.150146
Adjusted R Square	0.143401
Standard Error	3.575536
Observations	128

ANOVA

	df	*SS*	*MS*	*F*	*Significance F*
Regression	1	284.5923	284.5923	22.2608	6.22E-06
Residual	126	1610.842	12.78446		
Total	127	1895.434			

	Coefficients	*Standard Error*	*t Stat*	*P-value*	*Lower 95%*	*Upper 95%*	*Lower 95.0%*	*Upper 95.0%*
Intercept	9.273574	0.859828	10.78538	1.3E-19	7.571999	10.97515	7.571999	10.97515
Band width	3.876629	0.821644	4.718135	6.22E-06	2.250619	5.502638	2.250619	5.502638

Table 17. Regression model for increase in height and growth band width as growth variables during the 2nd complete year of growth.

Regression Statistics	
Multiple R	0.397286
R Square	0.157837
Adjusted R Square	0.150039
Standard Error	3.64855
Observations	110

ANOVA

	df	*SS*	*MS*	*F*	*Significance F*
Regression	1	269.4483	269.4483	20.24113	1.73E-05
Residual	108	1437.687	13.31192		
Total	109	1707.136			

	Coefficients	*Standard Error*	*t Stat*	*P-value*	*Lower 95%*	*Upper 95%*	*Lower 95.0%*	*Upper 95.0%*
Intercept	7.922277	0.749739	10.56672	2.39E-18	6.436165	9.408389	6.436165	9.408389
width	2.452071	0.545024	4.499014	1.73E-05	1.371739	3.532403	1.371739	3.532403

Table 18. Regression model for increase in height and growth band width as growth variables during the 3rd complete year of growth.

Regression Statistics	
Multiple R	0.555432
R Square	0.308504
Adjusted R Square	0.299639
Standard Error	2.786173
Observations	80

ANOVA

	df	*SS*	*MS*	*F*	*Significance F*
Regression	1	270.1358	270.1358	34.79894	8.92E-08
Residual	78	605.4952	7.762758		
Total	79	875.6309			

	Coefficients	*Standard Error*	*t Stat*	*P-value*	*Lower 95%*	*Upper 95%*	*Lower 95.0%*	*Upper 95.0%*
Intercept	4.466316	0.653897	6.830306	1.65E-09	3.164507	5.768124	3.164507	5.768124
width	2.809996	0.476346	5.899063	8.92E-08	1.861663	3.758328	1.861663	3.758328

Table 19. Kruskal–Wallis and Mann-Whitney pairwise tests output for ANOVA of temperature by site.

Kruskal-Wallis test for equal medians	
H (chi2):	50.74
Hc (tie corrected):	50.74
p (same):	7.83E-08
There is a significant difference between sample medians	

Mann-Whitney pairwise test U (in black) and p value (in red).										
N	523	513	515	509	495	502	481	530	505	435
	R13	R18	R31	R38	R48	R49	T3	T6	T7	R45
R13		0.485	0.652	0.488	0.228	0.005	0.000	0.171	0.951	0.002
R18	130788.5		0.288	0.892	0.057	0.001	0.000	0.546	0.612	0.000
R31	132493.5	127042		0.253	0.467	0.029	0.003	0.085	0.654	0.008
R38	129786.5	129917	125658		0.059	0.001	0.000	0.471	0.590	0.000
R48	123783.5	118162	124090.5	117292.5		0.145	0.014	0.014	0.279	0.038
R49	118059.5	112865	119052.5	111974	117619		0.327	0.000	0.009	0.508
T3	109713	105483	110262.5	104355	108279.5	116368.5		0.000	0.001	0.788
T6	131831	133005	128076	131399	119530	113821	106496		0.260	0.000
T7	131763	127155.5	127927.5	126008	120039.5	114786	106747.5	128414.5		0.002
R45	100233	95771.5	100836.5	95275.5	99199	106448	103540	97008	97241	

Table 20. Kruskal–Wallis and Mann-Whitney pairwise tests output for ANOVA of Secchi reading per sampling event.

Kruskal-Wallis test for equal medians	
H (chi2):	17.07
Hc (tie corrected):	17.09
p (same):	0.002
There is a significant difference between sample medians	

Mann-Whitney pairwise test U (in black) and p value (in red).					
N	10	10	10	10	10
	Apr-18	Jul-18	Jan-19	Apr-19	Jul-19
Apr-18		0.088	0.010	0.256	0.970
Jul-18	27		0.970	0.013	0.095
Jan-19	15.5	49		0.000	0.011
Apr-19	34.5	16.5	0.5		0.364
Jul-19	50	27.5	16	37.5	

Table 21. Table A-9. Kruskal–Wallis and Mann-Whitney pairwise tests output for ANOVA of Dissolved Oxygen, DO, (mg/l) per sampling event.

Kruskal-Wallis test for equal medians	
H (chi2):	63.47
Hc (tie corrected):	63.48
p (same):	5.37E-13
There is a significant difference between sample medians	

Mann-Whitney pairwise test U (in black) and p value (in red).					
N	20	20	20	20	20
	18-Apr	18-Jul	19-Jan	19-Apr	19-Jul
18-Apr		0.675	0.000	0.000	0.099
18-Jul	184		0.000	0.000	0.473
19-Jan	12	2		0.000	0.000
19-Apr	36	58.5	57.5		0.000
19-Jul	138.5	173	0	0	

Table 22. Kruskal–Wallis and Mann-Whitney pairwise tests output for ANOVA of shell size per sampling event.

Kruskal-Wallis test for equal medians	
H (chi2):	13.26
Hc (tie corrected):	13.26
p (same):	0.02103
There is a significant difference between sample medians	

Mann-Whitney pairwise test U (in black) and p value (in red).						
N	67	126	122	143	46	95
	Apr-18	Jul-19	Apr-19	Jul-18	Nov-18	Jan-19
Apr-18		0.526	0.090	0.228	0.524	0.397
Jul-19	3986		0.222	0.499	0.171	0.066
Apr-19	3477.5	6995		0.469	0.024	0.003
Jul-18	4295	8578.5	8272.5		0.069	0.008
Nov-18	1431.5	2501.5	2172	2702		0.981
Jan-19	2933	5118.5	4408	5413.5	2179	

Table 23. Kruskal–Wallis and Mann-Whitney pairwise tests output for ANOVA of shell size per site.

Kruskal-Wallis test for equal medians	
H (chi2):	64.99
Hc (tie corrected):	64.99
p (same):	1.45E-10
There is a significant difference between sample medians	

Mann-Whitney pairwise test U (in black) and p value (in red).										
N	93	71	79	103	24	79	93	52	3	2
	R49	R31	T6	R48	T3	R13	R38	T7	R45	R18
R49		0.665	0.000	0.006	0.024	0.004	0.000	0.000	0.354	0.037
R31	3170.5		0.000	0.029	0.043	0.009	0.000	0.000	0.468	0.082
T6	2006.5	1761		0.000	0.370	0.096	0.007	0.361	0.354	0.153
R48	3704	2943.5	2698		0.294	0.379	0.007	0.000	0.717	0.041
T3	782	615.5	832.5	1065		0.794	0.938	0.093	0.787	0.136
R13	2740.5	2109.5	2642	3758	914		0.489	0.012	0.941	0.124
R38	2563	2219.5	2792	3722	1104	3448		0.002	0.875	0.035
T7	1064	995	1859.5	1550.5	473	1517.5	1665		0.188	0.216
R45	95	79.5	80.5	135	32	115	131.5	42		0.149
R18	12	19	31.5	15.5	8	28	11	24.5	0	

Table 24. Table A-11. Kruskal–Wallis and Mann-Whitney pairwise tests output for ANOVA of MI per sampling event

Kruskal-Wallis test for equal medians	
H (chi2):	53.61
Hc (tie corrected):	53.61
p (same):	6.35E-11
There is a significant difference between sample medians	

Mann-Whitney pairwise test U (in black) and p value (in red).					
N	41	68	48	61	54
Median	17.66	19.65	20.13	24.22	23.47
	Apr-18	Jul-18	Jan-19	Apr-19	Jul-19
Apr-18		0.013	0.009	0.000	0.000
Jul-18	996		0.790	0.000	0.000
Jan-19	668	1584		0.000	0.000
Apr-19	453	1055	734		0.172
Jul-19	487	1119	771	1403	

Table 25. Kruskal–Wallis and Mann-Whitney pairwise tests output for ANOVA of MI per site.

Kruskal-Wallis test for equal medians	
H (chi2):	48.74
Hc (tie corrected):	48.74
p (same):	2.55E-08
There is a significant difference between sample medians	

Mann-Whitney pairwise test U (in black) and p value (in red).								
N	42	61	28	35	50	21	38	30
Median	17.68	22.01	19.74	22.33	20.22	19.73	23.94	23.84
	R38	R48	R13	R31	R49	T3	T6	T7
R38		0.000	0.025	0.000	0.000	0.004	0.000	0.000
R48	579		0.329	0.311	0.063	0.807	0.079	0.018
R13	400	743		0.110	0.963	0.425	0.044	0.013
R31	329	934	374		0.027	0.426	0.687	0.403
R49	593	1211	695	627		0.525	0.003	0.000
T3	242	617	254	320	474		0.232	0.094
T6	294	914	376	628	591	323		0.762
T7	130	635	259	461	357	227	545	

Table 26. Kruskal–Wallis and Mann-Whitney pairwise tests output for ANOVA of length: height ratio per site.

Kruskal-Wallis test for equal medians	
H (chi2):	80.98
Hc (tie corrected):	81.23
p (same):	7.72E-15
There is a significant difference between sample medians	

Mann-Whitney pairwise test U (in black) and p value (in red).								
N	79	71	93	103	93	24	79	52
	R13	R31	R38	R48	R49	T3	T6	T7
R13		0.047	0.295	0.015	0.007	0.659	0.000	0.001
R31	2278		0.003	0.000	0.000	0.539	0.050	0.102
R38	3333	2393.5		0.148	0.084	0.356	0.000	0.000
R48	3210.5	2185.5	4217		0.647	0.073	0.000	0.000
R49	2794.5	1934.5	3691.5	4608		0.079	0.000	0.000
T3	891	780	979	945.5	856		0.068	0.119
T6	2030.5	2283.5	2106	1828	1701	714.5		0.828
T7	1351	1527	1400.5	1201.5	1088.5	484.5	2007.5	

Table 27. Kruskal–Wallis and Mann-Whitney pairwise tests output for ANOVA of length: width ratio by site.

Kruskal-Wallis test for equal medians	
H (chi2):	68.21
Hc (tie corrected):	68.27
p (same):	3.30E-12
There is a significant difference between sample medians	

Mann-Whitney pairwise test U (in black) and p value (in red).								
N	79	71	93	103	93	24	79	52
	R13	R31	R38	R48	R49	T3	T6	T7
R13		0.205	0.001	0.934	0.000	0.673	0.017	0.348
R31	2467.5		0.065	0.211	0.001	0.607	0.001	0.053
R38	2614.5	2746		0.001	0.067	0.055	0.000	0.000
R48	4039	3247.5	3420		0.000	0.633	0.007	0.282
R49	2158.5	2312	3652.5	2846.5		0.003	0.000	0.000
T3	893.5	791.5	831.5	1158	681		0.023	0.202
T6	2434.5	1882.5	1874	3121	1571.5	656.5		0.297
T7	1854	1467	1536.5	2393.5	1317.5	509.5	1832	

Table 28. Kruskal–Wallis and Mann-Whitney pairwise tests output for ANOVA of shell weight: total dimensions (shell index) by site.

Kruskal-Wallis test for equal medians	
H (chi2):	51.71
Hc (tie corrected):	51.71
p (same):	5.12E-08
There is a significant difference between sample medians	

Mann-Whitney pairwise test U (in black) and p value (in red).										
N	35	1	36	50	1	61	50	21	40	35
	R13	R18	R31	R38	R45	R48	R49	T3	T6	T7
R13		0.178	0.128	0.168	0.773	0.721	0.039	0.310	0.480	0.100
R18	3		0.122	0.096		0.094	0.096	0.115	0.099	0.102
R31	497	1		0.934	0.963	0.334	0.584	0.065	0.037	0.009
R38	720	0	890		0.865	0.003	0.642	0.000	0.000	0.000
R45	14	0	17	22		0.342	0.973	0.207	0.331	0.124
R48	1020	0	968	1016	13		0.015	0.029	0.004	0.000
R49	643	0	837	1182	24	1114		0.001	0.000	0.000
T3	307	0	266	206	2	435	262		0.958	0.335
T6	633	0	519	465	8	807	511	416		0.500
T7	472	0	402	219	1	543	335	310	636	